

**SELECTIVE AND REGULATED RF HEATING
OF STENT TOWARD ENDOHYPERThERMIA
TREATMENT OF IN-STENT RESTENOSIS**

by

Yi Luo

B.A.Sc, University of Regina, 2012

A THESIS SUBMITTED IN PARTIAL FULFILLMENT OF
THE REQUIREMENTS FOR THE DEGREE OF

MASTER OF APPLIED SCIENCE

in

The Faculty of Graduate and Postdoctoral Studies

(Electrical and Computer Engineering)

THE UNIVERSITY OF BRITISH COLUMBIA

(Vancouver)

December, 2014

© Yi Luo, 2014

Abstract

This thesis presents a novel active stent system with a selective radio frequency (RF) heating and temperature regulation capabilities. Such system is targeted at the application to endohyperthermia treatment for in-stent restenosis problems, providing a cheap and non-invasive long-term solution to the blood vessel blockage caused by a growth of scar tissue across the stent structure after implantation.

The research work consists of two major portions. Firstly, a novel active stent device with ability of selective RF heating has been custom designed and explored. The device is formed by integrating a stainless-steel based stent with a flexible capacitor strip, which serves as a frequency-selective wireless heater controlled using a tuned RF electromagnetic field applied externally. The proof-of-concept prototype device has been developed based on micro-electromechanical systems (MEMS) fabrication processes; its electrical and thermal characteristics are studied thoroughly. The finalized device is tested and evaluated within an artificial artery for validating its potential feasibility of wireless stent hyperthermia.

Secondly, a MEMS-based, thermally sensitive circuit breaker chip has been designed and fabricated for the active stent temperature regulation. The temperature of an active stent device can be managed within a certain range after integrated with the chip, offering the controllability of RF heating of the device. Customized design and packaging methods are used in the chip fabrication; the chip-stent integration technique is also explored. The finalized device is evaluated with *in-vitro* tests, showing its temporal capability and wireless reliability. The experiment result verifies device working principles and suggests a direction of future research on non-invasive endohyperthermia treatments for long-term restenosis management.

Preface

The thesis contains my research works and discusses all experiments, simulations, and results verification conducted in Takahata Lab at the University of British Columbia Vancouver campus under the direct supervision of Prof. Kenichi Takahata. All device fabrication works are performed at the Advance Materials Process and Engineering Laboratory (AMPEL) and the Takahata Lab at UBC Vancouver campus with a financial support from Canadian Microelectronics Corporation (CMC). I contributed following publications as the first author while writing most of the manuscript contents with review and revision by Prof. Kenichi Takahata and co-authors. Conference paper 1 and journal paper 1 cover the contents in Chapter 2, conference paper 2 and journal paper 2 cover the contents in Chapter 3, and journal paper 3 cover the contents in Chapter 4. The circuit breaker design to be discussed partly followed the previous design of a MEMS contact switch developed by Dr. Masoud Dahmardeh for further development. The stainless-steel inductive stent described in this thesis was designed by Dr. Xing Chen.

Conference papers:

1. Y. Luo, M. Dahmardeh, X. Chen and K. Takahata, "Selective RF Heating of Resonant Stent toward Wireless Endohyperthermia for Restenosis Inhibition," *27th IEEE Int'l Conf. Micro Electro Mechanical Systems (MEMS 2014)*, San Francisco, USA, January 2014, pp. 877-880.
2. Y. Luo, M. Dahmardeh and K. Takahata, "Biocompatible Circuit-Breaker Chip for Temperature Regulation of Electrothermally Driven Smart Implants," *28th IEEE Int'l Conf. Micro Electro Mechanical Systems (MEMS 2015)*, Estoril, Portugal, January 2015, accepted.

Journal papers:

1. Y. Luo, M. Dahmardeh, X. Chen and K. Takahata, "Radiofrequency Resonant Stent for Wireless Endohyperthermia Treatment of Restenosis," Submitted to a peer-reviewed journal.

2. Y. Luo, M. Dahmardeh and K. Takahata, “Biocompatible Circuit-Breaker Chip for Thermal Management of Biomedical Microsystems,” Submitted to a peer-reviewed journal.
3. Y. Luo, X. Chen, M. Dahmardeh and K. Takahata, “RF-Powered Stent with Integrated Micro Circuit Breaker for Safeguarded Wireless Hyperthermia Treatment of In-Stent Restenosis,” to be submitted to a peer-reviewed journal.

Table of Contents

Abstract	ii
Preface	iii
Table of Contents	v
List of Tables	vii
List of Figures	viii
Acknowledgements	xiii
Dedication	xiv
1 Introduction	1
1.1 The stent: present art and challenges	1
1.1.1 The medical coronary stent.....	1
1.1.2 The in-stent restenosis.....	3
1.2 Advanced stent technology	5
1.2.1 “Active stent” for wireless endohyperthermia	5
1.2.2 Stent temperature regulation	6
1.3 Thesis composition	7
2 Selective RF Resonant Stent Device	8
2.1 Device principle and design	8
2.2 Device fabrication	11
2.3 Experimental results	13
2.3.1 The medical coronary stent.....	13
2.3.2 The medical coronary stent.....	15
2.3.3 The medical coronary stent.....	18
3 Biocompatible Circuit-breaker Chip for Thermal Management	28
3.1 The thermal sensitive MEMS actuator design	29
3.2 Chip based circuit breaker device design	31
3.3 Chip fabrication	33
3.4 Device characterization	36
3.4.1 The medical coronary stent.....	37
3.4.2 The medical coronary stent.....	38

3.4.3	The medical coronary stent.....	41
4	The Active Stent with Temperature Regulation	45
4.1	Working principle and device design	45
4.2	Fabrication	48
4.3	Experimental results and discussion	50
4.3.1	Device expansion	50
4.3.2	Experimental results and discussion	50
4.3.3	RF heating tests	53
5	Conclusion and Future Outlook	63
5.1	Conclusion	63
5.2	Contributions	65
5.3	Future outlooks	66
	Bibliography.....	68

List of Tables

Table 2.1	Values of electrical parameters measured with fabricated active stent at three different expansion conditions	16
Table 3.1	The specification of the circuit-breaker chip applied for fabrication	33
Table 4.1	Values of electrical parameters of fabricated active circuit-breaker stent at three different expansion conditions	52

List of Figures

Figure 1.1 The concept of angioplasty of stent placement. (a) The location of coronary artery; (b) the unexpanded stent carried by an angioplasty balloon catheter inserted into the narrowed artery; (c) the stent is expanded by the balloon catheter, compressing the plaque against to artery wall; (d) the artery is widened by the expanded stent. (Source: National Heart, Lung, and Blood Institute, with permission).....2

Figure 1.2 The formation of restenosis. (a) The location of coronary artery where the stent implanted; (b) the widened artery with normal blood flow; (c) restenosis appears through and around the stent over time. (Source: National Heart, Lung, and Blood Institute, with permission)4

Figure 2.1 The conceptual drawing of a novel stent with high frequency selectivity controlled using external RF fields to wireless endohyperthermia for in-stent restenosis10

Figure 2.2 Design of the proof-of-concept device: (a) Top view of the capacitor strip; (b) and (c) respectively top and side views of the stent coupled with the capacitor strip forming an *LC* circuit as displayed in (c)11

Figure 2.3 Fabrication process for active stent prototype12

Figure 2.4 Fabrication and expansion results: (a) Fabricated device before expansion. (b) The device mounted on a 4mm balloon catheter. (c) The device expanded with the balloon up to 6mm in diameter inside artificial artery tube. (d) The fully expanded stent device within the artificial artery14

Figure 2.5 Measured device resonance frequencies and Q factors: (a) Resonant dips in impedance phase of reader antenna and (b) Q factors of the device at different expansion conditions measured as a function of frequency.....16

Figure 2.6 Device EMF measurement: (a) EMF waveforms generated in the partially expanded stent device due to RF excitation. (b) Measured EMF amplitude as a function of field frequency and (c) distance between antenna and device (at resonance)17

Figure 2.7	Experimental set-up used for wireless heating tests	18
Figure 2.8	Measured thermal responses of stent device located through the antenna loop: (a) Temporal behaviour of stent temperatures (at the center and edge regions) with RF switching, and (b) generated temperature vs. field frequency observed in the unexpanded device, and (c)-(d) those observed in the fully expanded device inside the artificial artery	21
Figure 2.9	IR images of stent device located through the antenna loop before expansion: (a) without and (b) with RF excitation and the device fully expanded inside the artificial artery (c) without and (d) with the excitation implemented using the identical RF output power	22
Figure 2.10	Measured thermal responses of stent device located in parallel with the antenna loop: (a) Temporal behaviour of stent temperatures (at the center and edge regions) with RF switching, and (b) generated temperature vs. field frequency observed in the unexpanded device, and (c)-(d) those observed in the fully expanded device inside the artificial artery	24
Figure 2.11	IR images of stent device located in parallel with the antenna loop before expansion: (a) without and (b) with RF excitation and the device fully expanded inside the artificial artery (c) without and (d) with the excitation made using the same RF output power	25
Figure 2.12	Generated temperature vs. device-antenna distance measured with the fully expanded device	26
Figure 3.1	Conceptual illustration of the circuit-breaker chip and its application for temperature regulation of wireless “smart” implant such as implantable drug-delivery device driven by RF-powered micro heaters or electrothermal actuators.....	28
Figure 3.2	A cantilever model of the bimorph SMA actuator used for the circuit-breaker device showing (a) dimensional parameters of the structure and (b) other parameters relevant to the bent condition of the cantilever	30
Figure 3.3	The proposed bimorph cantilever structure: (a) Design of Nitinol SMA cantilever actuator for the circuit breaker and (b) FEA simulation for	

	displacement of the cantilever with SiO ₂ reset layer indicating a downward free-end displacement of 174.3 μm at room temperature	31
Figure 3.4	Developed process for the fabrication of the circuit-breaker chip	35
Figure 3.5	Fabrication results: (a) Completed circuit-breaker chip; (b) Nitinol actuator component patterned using μEDM; SEM images of (c) Nitinol switch and (d)-(e) close-ups of the switch structure (locations indicated in Figure 3.5(c))	36
Figure 3.6	Measured temporal behaviour of free-end displacement of the Nitinol cantilever with temperature increase applied to the cantilever	38
Figure 3.7	Electrical contact resistances of (a) standalone fabricated breaker switch (without Ti packaging) and (b) completed circuit-breaker chip (with Ti packaging) recorded as a function of temperature in a cycle of heating and cooling	40
Figure 3.8	Self-heating effects of fabricated circuit-breaker chip observed by application of (a) DC and (b) RF signals fed to the chip	40
Figure 3.9	Experimental set-up used for wireless heating tests with an RF resonant heater	42
Figure 3.10	Measured thermal response of the circuit-breaker-coupled wireless heater showing self-regulated on-off cycle of the breaker chip and resultant temperature regulation observed in the heating inductor. The behaviour of the heater without the circuit breaker is also plotted for comparison.....	44
Figure 4.1	Endohyperthermia treatment of in-stent restenosis through the active <i>LC</i> -tank stent with the integrated MEMS circuit breaker that serves as a wireless heater with an absolute temperature limiter. Once implanted, the device is activated by resonating it using an externally applied RF electromagnetic field to perform the thermal therapy	47
Figure 4.2	The fabrication process of the active stent with circuit breaker chip	48
Figure 4.3	Fabricated active stent device (top) with close-up views of the integrated circuit-breaker chip (left) and the other side of the stent terminal on which the interconnect wire was bonded (right)	49

Figure 4.4	Expansion test results: (a) Fabricated device mounted on a deflated 4-mm balloon catheter before expansion (left) and after expansion by inflating the balloon at 12 atm (as shown in the pressure meter of the inflator) (right); (b) the partly expanded device mounted on a deflated 6-mm balloon catheter and positioned inside artificial artery with 6-mm diameter (top) and expanded by balloon inflation (bottom); (c) side (left) and axial (right) views of the stent device fully expanded within the artificial artery	51
Figure 4.5	Measurement results: (a) Measured shifts of resonant dips in impedance phase of reader antenna led by expansion process, and (b) Q factors of the device recorded as a function of frequency at different expansion conditions	53
Figure 4.6	Measured temperatures of the stent device located through the antenna loop measured at the maximum temperature point of the stent as well as on the integrated circuit-breaker chip: (a) Temporal behaviour of the temperatures with RF switching and (b) generated temperatures vs. field frequency recorded with the unexpanded device; (c) and (d) those recorded with the partially expanded device; (e) and (f) those recorded with the artificial artery containing the fully expanded device. The reference data recorded without circuit-breaker function is also shown in (c)-(f)	56
Figure 4.7	IR images of the stent device located through the antenna loop: (a) partially expanded device without RF excitation (top), with RF excitation at resonance (middle), and with RF excitation +20-MHz off the resonance (bottom); (b) artificial artery containing fully expanded device without RF excitation (top), with RF excitation at resonance (middle), and with RF excitation +12-MHz off the resonance (bottom). All RF excitations were performed with an identical RF output power (of 320 mW)	57
Figure 4.8	Measured temperatures of the stent device located in parallel with the antenna loop measured at the maximum temperature point of the stent as well as on the integrated circuit-breaker chip: (a) Temporal behaviour of the temperatures with RF switching and (b) generated temperatures vs.	

field frequency recorded with the partially expanded device; (c) and (d) those recorded with the artificial artery containing the fully expanded device. The reference data recorded without circuit-breaker function is also shown in each case.....58

Figure 4.9 IR images of the stent device located in parallel with the antenna loop: (a) partially expanded device without RF excitation (top), with RF excitation at resonance (middle), and with RF excitation +13-MHz off the resonance (bottom); (b) artificial artery containing fully expanded device without RF excitation (top), with RF excitation at resonance (middle), and with RF excitation +15-MHz off the resonance (bottom). All RF excitations were performed with an identical RF output power (of 320 mW)59

Figure 4.10 Results from wireless heating test of the active and control artificial arteries filled with liquid and RF excited: (a) Temporal thermal behaviours of the arteries filled with 0.15-M saline excited for 200 seconds; (b) and (c) IR images of the saline-filled active and control arteries, respectively, under RF radiation at 1.26-W output power (the timings that these images were recorded are indicated in (a) with arrows); (d) and (e) those of the DI-water-filled active and control arteries, respectively, under the same RF radiation62

Acknowledgements

I would like to take this opportunity to acknowledge the people who have been continuously guiding me throughout my entire M.A.Sc program. Firstly, I owe particular thanks to my program supervisor, Professor Kenichi Takahata, for his instrumental support and research supervision. It is my privilege to study, to work, to publish original research work in his lab, and to develop multidiscipline scientific skills and critical engineering thinking for my future professional career. Secondly, I offer my enduring gratitude to the faculty and staff in the Department of Electrical and Computer Engineering for the educational opportunity. It was a great experience of joining in, contributing to, and sharing with all members in the ECE society. Thirdly, I would acknowledge members of the AMPEL laboratory, Dr. Mario Beaudoin and Dr. Alina Kulpa, and fellow members in the Takahata lab, Dr. Xing Chen, Dr. Zhiming Xiao, Dr. Masoud Dahmardeh, Babak Assadsangabi, Dan Brox, Jeffrey Fong, Akio Taniguchi, and Saquib Mirza. My work would be impossible without their technical supports and coherent answers to my questions. Finally, my special thanks are owed to the committee members, Prof. Boris Stoeber and Prof. John Madden, who helped in my thesis revision and shared their experience to enlarge my vision of engineering, and also to my family members, who have supported me throughout my course of education, both morally and financially.

Dedication

To my beloved family...

Chapter 1

Introduction

This chapter presents the background information of my research project. Starting with a thoroughly introduction of coronary stent, the problem of in-stent restenosis and the solution of active stent proposed in this project are discussed in section 1.1. Section 1.2 presents the requirement of temperature regulation for active stents and the proposed solution. This chapter ends with the outline of this thesis in section 1.3.

1.1 The stent: present art and challenges

1.1.1 The medical coronary stent

Coronary artery related cardiovascular disease is currently one of the most common causes of death in North America [1]. It leads patients suffer from symptoms like high blood pressure, irregular heartbeat and heart attacks due to the progressive narrowing of the coronary artery caused by stenosis formation on the artery wall. Currently, coronary stent implantation is the most frequently suggested treatment for patients suffering from cardiovascular disease. Each year, over three million stents are implanted by percutaneous coronary intervention worldwide, for both vascular (e.g., coronary, carotid, renal, and peripheral arteries) and non-vascular (e.g., urinary and biliary ducts) applications [2]. Most of commercialized stents have tubular bodies of stainless steel or shape memory alloy (SMA), which are designed to be expanded radially in order to physically scaffold diseased sites of arteries narrowed by atherosclerosis, i.e., plaque deposition on the vessel walls [3]. Shown in Figure 1.1 is the typical procedure of

angioplasty of stent placement by percutaneous coronary intervention [4]. The pre-expansion stent is crimped on a deflated balloon catheter and delivered to the desired portion of the diseased vessel with the help of x-ray imaging using contrast dye injection [5]. With the balloon dilatation, the stent would be expanded and compressing the plaque against to artery wall. Hence the artery inner wall is supported by the expanded stent to prevent path blockage. After placing the stent, the balloon catheter is deflated again and retreated out of body, while the stent scaffolds the inside of the artery vessel to continuously widen the blood path.

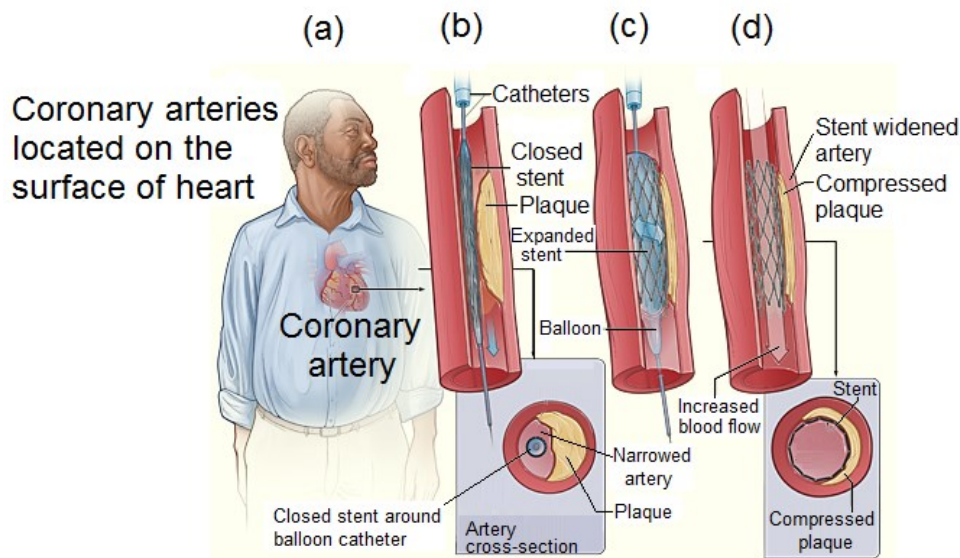


Figure 1.1: The concept of angioplasty of stent placement. (a) The location of coronary artery; (b) the unexpanded stent carried by an angioplasty balloon catheter inserted into the narrowed artery; (c) the stent is expanded by the balloon catheter, compressing the plaque against to artery wall; (d) the artery is widened by the expanded stent. (Source: National Heart, Lung, and Blood Institute, with permission)

There are several advantages of using stent implantation. Firstly, this treatment does not require an open-heart surgery such as the coronary artery bypass grafting (CABG). All procedures are performed with a tiny cut open for coronary catheter intervention, which

significantly reduces the chance of infection. Secondly, stent implantation does not need a general anesthesia. Patients stay awake during the procedure, with almost no side effect from anesthetic medicine. Moreover, stent treatment has much shorter recovery time. Patients stay in a special care unit only for few hours after the stent implantation to ensure blood pressure, heartbeat rate, body temperature, and oxygen level stay normal. In some cases, however, for people who have several coronary heart diseases or poor functional left heart chamber, stent implantation turns to be risky while CABG would be a safer option.

1.1.2 The in-stent restenosis

Although stent implantation is effective in atherosclerosis treatment, a long-term complication called restenosis, or re-narrowing of blood vessels, occurs in stented patients with substantial rates (e.g., up to 60% [6]), mainly due to scar-tissue proliferation within the stent. When severe, it may lead to complete blockage of blood flow again over time and relapsing cardiovascular diseases [7]. As shown in Figure 1.2, the diseased artery reestablished its normal blood flow right after the stent implantation; blood path is widened by an expanded stent scaffolds to the artery wall [4]. When tissues start to progressively grow through and around the implanted stent, the blood path narrows and results in abnormal blood flow again.

To inhibit the problematic restenosis growth, a type of stent called drug-eluting stent (DES) was invented and had been commercialized for clinical usage [8], [9]. Comparing with bare metal stent, this stent is coated with specific restenosis restraint medicine. After normal stent implantation, the coated medicine would be gradually released to reduce the

growth of scar tissue around the stent. In this manner, restenosis growth is manageable by using a variety of medicine coating; however, this is the case only before the medicine is used up. Also, in-stent thrombosis (blood clot) might be introduced by implanting DESs [10]. Hence, at present stage, DES is neither a permanent nor a premium solution for solving the problem of restenosis. Recently, studies in hyperthermia treatments of restenosis have shown that moderate heating of stent (to temperatures of ~ 50 °C) is effective in limiting cell proliferation without thrombosis induction [11]. This promising result was, however, obtained using a special catheter to heat a stent, requiring an invasive procedure that not only limits the implementation of the method but also increases the treatment cost.

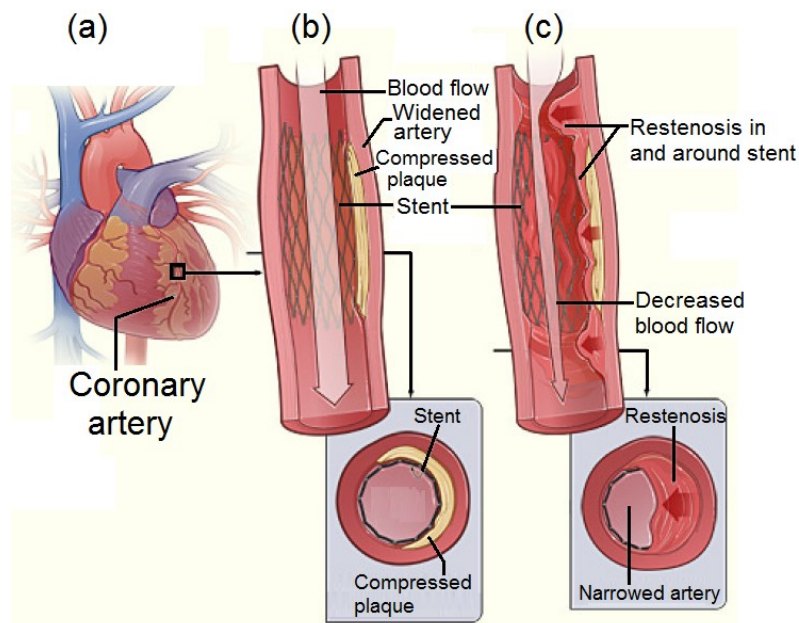


Figure 1.2: The formation of restenosis. (a) The location of coronary artery where the stent implanted; (b) the widened artery with normal blood flow; (c) restenosis appears through and around the stent over time. (Source: National Heart, Lung, and Blood Institute, with permission)

1.2 Advanced stent technology

1.2.1 “Active stent” for wireless endohyperthermia

Unlike other implantable sensory devices powered by implanted batteries [12], [13], this project explores a novel method and technology to wirelessly control heating of implanted stents. The aim is to offer a reliable therapeutic mean of stent-based wireless endohyperthermia towards long-term prevention and management of restenosis, an inherent issue involved in the implantation of present stents including DESs [14]. The benefit of this device is that it provides efficient and controllable local heating in a vessel or body conduit where a stent could be implanted. Wireless MEMS devices have been reported to utilize inductor-capacitor (*LC*) resonant circuits as wireless heaters controlled using external RF fields for the actuation of thermoresponsive microstructures [15], [16]. The resonant heaters have been demonstrated to provide efficient RF-to-thermal energy conversion and high frequency selectivity in heating, enabling low-power and precision wireless RF operation of the devices performed by modulating the frequency of the external field. This wireless heating mechanism is applied to develop the wireless active stent by constructing the stent to form an *LC*-tank circuit. When implanted, the device fully deploys the tank circuit to function as a frequency-sensitive wireless heater. By tuning an external field radiated to the implanted device through the skin, the device is precisely activated to locally apply heat stress to inhibit neointimal hyperplasia, the major cause of in-stent restenosis [11]. The efficient resonant heating principle is expected to enable precision control of wireless thermal treatment while suppressing the RF radiation power exposed to the body.

1.2.2 Stent temperature regulation

As a device designed for hyperthermia treatment, temperature regulation is mandatory to prevent high temperature that causes destructions to healthy cells and tissue in addition to killing diseased cells and tissue. Studies have indicated that moderate heating of stent is effective for inhibiting neointimal hyperplasia [11], while enzyme activities are massively affected when the temperature rises higher than 50 °C [17]. The function of temperature regulation can be achieved by using a wide range of temperature sensing and electrothermal triggering mechanisms. The present technology exploits multifunctional microsystems such as MEMS transducers as a practical avenue to realize electrothermally active stent devices with temperature regulation and control functions, enabling safe, reliable operation of endohyperthermia treatment of vascular diseases including restenosis problems.

In this study, an electro-thermal MEMS circuit breaker is integrated on the inductive stent, in order to physically limit heating of the stent within a designed threshold temperature. The circuit breaker is designed to serve as a threshold temperature sensitive actuator. The actuator would be formed in a form of cantilever structure. It will switch on/off the electrical contact depending on temperature without requiring any external power source. The cantilever is formed using SMA, a temperature-sensitive material, which has a threshold temperature close to the temperature potentially usable for hyperthermia treatment (45-50 °C) to be performed with the active stent. When the stent temperature is below the threshold temperature, the circuit breaker maintains its closing state and continuously conducts current for stent heating. Once the stent temperature rises to the threshold temperature, the cantilever deforms and opens the electrical connection, turning

the device to the off state. Once the stent temperature decreases below the threshold temperature, the breaker returns to the on state to restore the circuit and resume heating. Consequently, this device passively regulates its temperature enabled by the integration of the micro circuit breaker with the *LC* circuit of the inductive stent.

1.3 Thesis composition

In this thesis, the selective RF resonant stent device design and characterization are discussed in detail in chapter 2. The prototype device fabrication process and all experiment results are demonstrated and concluded as the first stage of this project. The second project phase starts with the design and characterization of the SMA actuator for the circuit breaker, followed by the fabrication process with a chip based packaging and the device integration with the stent for device circuitry formation, which are discussed in chapter 3. The active stent with a temperature regulation capability is discussed in chapter 4. The study of stent heating with temperature regulation is followed with an *in-vitro* test; the thermal capability of the device is evaluated for its clinical potential. Contents in chapter 5 conclude all studies and experiments in this project; future directions of research are suggested for further study.

Chapter 2

Selective RF Resonant Stent Device

This chapter introduces the first phase of the project; a research on an electrothermally active stent targeted at the application to endohyperthermia treatment for in-stent restenosis problems [18]. The stainless-steel stent designed to function as an electrical inductor is integrated with a flexible capacitor strip to form a passive resonant circuit, which serves as a frequency-selective wireless heater controlled using a tuned RF electromagnetic field applied externally. The working principle and device design are stated in section 2.1. The fabrication process and result are shown in section 2.2, which is followed by device characterization experiments and RF heating tests in section 2.3.

2.1 Device principle and design

The proposed active stent is constructed by electromechanically coupling an inductive stent [19] with a planar capacitive element to establish an LC circuit that behaves as the wireless resonant heater. An AC current is generated in the circuit when exposed to an AC magnetic field due to the electromotive force (EMF) induced by the field. The reactance of the circuit becomes zero when the frequency of the magnetic field, f_m , matches the resonant frequency of the circuit, f_r , expressed as $(2\pi\sqrt{LC})^{-1}$, where L and C are the inductance and capacitance of the circuit, respectively. At this condition, the power transfer to the stent circuit, P_s , is maximized, leading to the following condition [20]:

$$P_{S_max} = P_S \Big|_{f_m=f_r} = \frac{v^2}{R} \quad (2.1)$$

where v is the EMF and R is the parasitic resistance of the circuit. Thus, the field power is most effectively converted to Joule heat in the inductive component of the circuit, the inductive stent, when the field frequency is tuned to f_r , exhibiting a strong dependence of heating on the field frequency. The theoretical steady-state temperature rise of the LC circuit, or the active stent based on the circuit, T_{ss} , can be described as [21]:

$$T_{ss} = \frac{R_T v^2 / R}{1 + \alpha_R R_T v^2 / R} \quad (2.2)$$

where R_T is the thermal resistance to the surrounding of the circuit and α_R is the temperature coefficient of resistance of the circuit. More discussion on the receiver coil power consumption can be found in [22]. Targeting at stent heating to temperatures up to 45-50 °C, the stent device/system should be configured to achieve the maximum T_{ss} of 8-13 °C assuming the body temperature of 37 °C.

For the stent device developed in this study, the f_r level of the device changes as the device is expanded and implanted in a blood vessel (refer to Figure 2.1). This change of frequency can be caused by different factors, including a change in the inductance of the stent due to a radial expansion of its structure (discussed in section 2.3) and capacitive effects due to the change of device ambient (from air to blood). Therefore, it will be important to determine the final f_r after the implantation. This determination can be performed through a well-established wireless technique, i.e., inductively coupling an external coil antenna with the inductive stent through the skin and detecting a dip in the

impedance of the antenna using a spectrum analyzer, where the dip frequency represents the f_r of the device [20]. Once this process is completed, the connection of the above antenna can be switched to a field generator to perform a tuned, resonant excitation of the device.

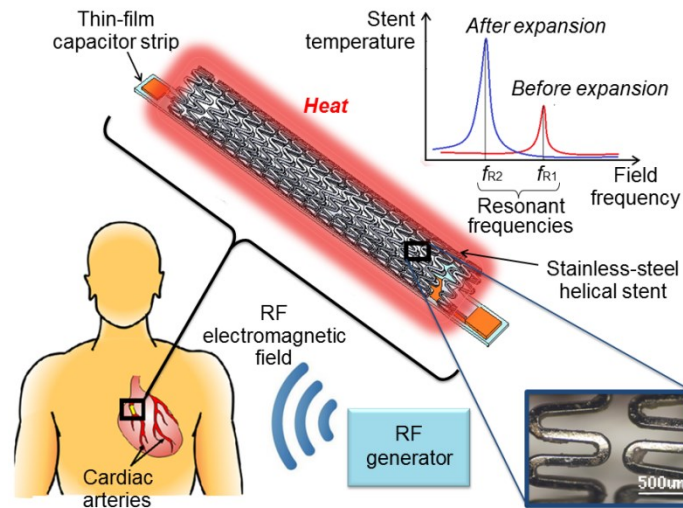


Figure 2.1: The conceptual drawing of a novel stent with high frequency selectivity controlled using external RF fields to wireless endohyperthermia for in-stent restenosis.

The inductive stent is fabricated by laser micromachining of medical-grade (type 316L) stainless-steel tubing (2.0-mm outer diameter, 100- μ m wall thickness) followed by electropolishing [23], the fabrication approach commonly used in the stent industry. The design of the proof-of-concept prototype developed is shown in Figure 2.2. The stent is fabricated to have a solenoid-like geometry, with 17 turns of meandering wire, as its overall shape so that it works as an electrical inductor that can be radially expanded using an angioplasty balloon [19]. To establish the *LC*-tank stent, the inductive stent is integrated with a planar capacitor, which is formed to have two Cu electrodes built on top and bottom of a thin, flexible polyimide (PI) film in a form of narrow strip (Figure 2.2).

This strip, providing a capacitance of ~ 2.9 pF with its design, is coupled with the inductive stent using the bonding terminals created at both ends of the stent. The top capacitor electrode is connected to a bonding pad on the bottom of the strip through a via so that single-sided bonding of the strip establishes its electrical connection to the stent.

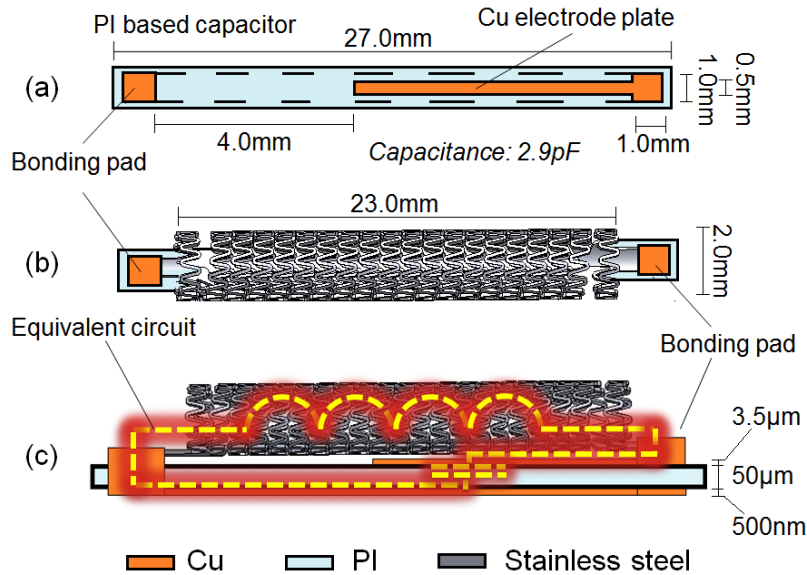


Figure 2.2: Design of the proof-of-concept device: (a) Top view of the capacitor strip; (b) and (c) respectively top and side views of the stent coupled with the capacitor strip forming an LC circuit as displayed in (c).

2.2 Device fabrication

Figure 2.3 shows the process flow developed for the prototype fabrication. The planar capacitor strip is fabricated using single-sided Cu-clad PI film with a thickness of $50\ \mu\text{m}$. The Cu-clad layer with $4\text{-}\mu\text{m}$ thickness on the PI film is photolithographically patterned by wet etching using a dry-film photoresist (SF-306, MacDermid Co. CO, USA) as a mask to create the top capacitor electrode (Figure 2.3, step (a)). The other Cu electrode (500-nm thick) is formed on the other side of the film by evaporating Cu through a litho-

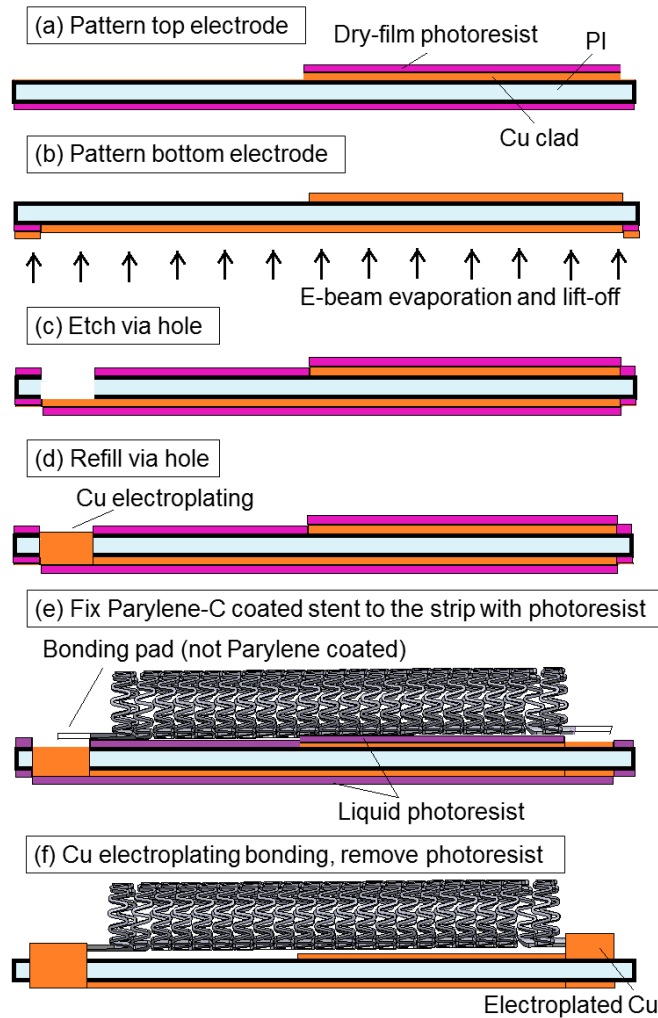


Figure 2.3: Fabrication process for active stent prototype.

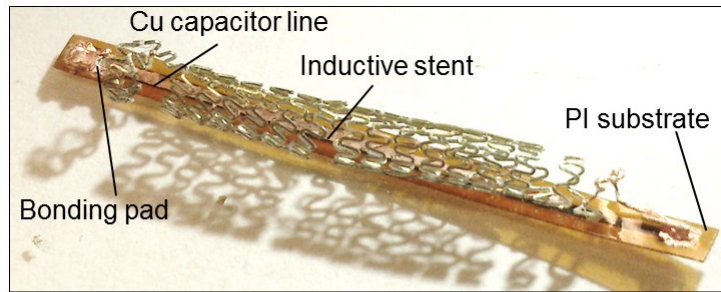
graphically patterned mask followed by a lift-off process (Figure 2.3, step (b)). Next, the via contact is formed in the PI film by wet etching of PI using a KOH-based solution (Figure 2.3, step (c)) and then refilling the hole with Cu electroplating (Figure 2.3, step (d)) [24]. Before performing the stent-capacitor bonding process, the stent is uniformly coated with Parylene C (Specialty Coating Systems Inc., IN, USA) for a thickness of 8 μm for electrical insulation except for the end terminals. After temporarily fixing the stent onto the capacitor strip using spin-coated liquid photoresist (SPR 220-7, Rohm and

Hass Co., PA, USA) and hard baking it for 4 hours at 120 °C (Figure 2.3, step (e)), Cu electroplating is again performed for 2 hours to electromechanically bond the stent's end terminals to the strip's bonding pads; dissolving all photoresist layers completes the fabrication (Figure 2.3, step (f)). The fabricated device is shown in Figure 2.4(a).

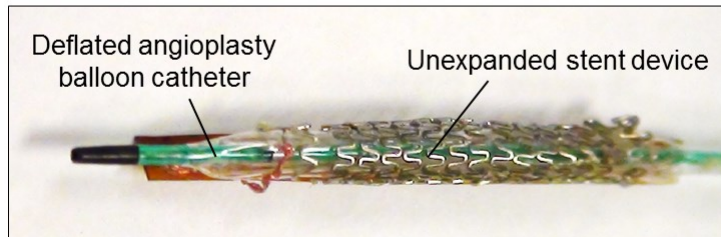
2.3 Experimental results

2.3.1 Device expansion

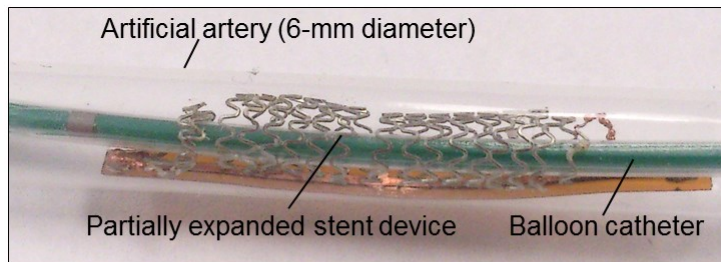
The expansion test of fabricate stent device was performed using commercial angioplasty balloon catheters (e.g., Advance®18LP Low Profile PTA Balloon Dilatation Catheter, Cook Medical Inc., IN, USA). To evaluate device response with different expansion conditions, the tests were implemented using the catheters with two different balloon diameters, i.e., 4 mm and 6 mm. The prototype was first expanded partially from original 2 mm to 4 mm in diameter using the 4-mm balloon catheter on which the unexpanded stent device was mounted (Figure 2.4(b)). After characterizing the partially expanded device, it was further expanded up to 6 mm in diameter using the 6-mm balloon catheter (Figure 2.4(c)). In each expansion, the pressure inside the balloon was increased to 13-15 atm, deforming the solenoid-like stent coil along the cylindrical shape of the balloon. Once the target diameter was reached, the balloon pressure was reduced toward zero to release the stent structure, followed by retrieving the catheter from the expanded stent. The expansion to the final 6-mm diameter was successfully performed inside a silicone-based artificial artery with 6 mm in diameter (Dynatek Labs, MO, USA) as displayed in Figure 2.4(d).



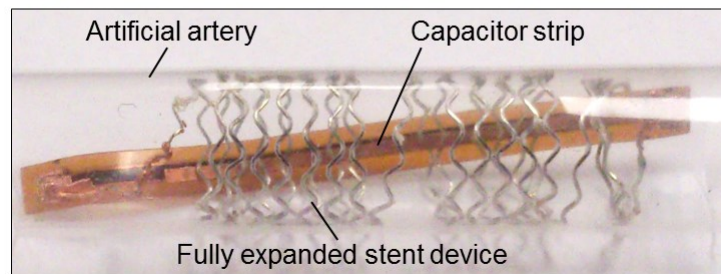
(a)



(b)



(c)



(d)

Figure 2.4: Fabrication and expansion results: (a) Fabricated device before expansion. (b) The device mounted on a 4mm balloon catheter. (c) The device expanded with the balloon up to 6mm in diameter inside artificial artery tube. (d) The fully expanded stent device within the artificial artery.

2.3.2 Device electromechanical characterization

As noted earlier, the inductance and resonant frequency of the device depend on the radial size to which the stent is expanded. This dependence was first characterized, by expanding the device in a manner described above, while wirelessly monitoring the resonant frequency of the device through the inductive coupling technique described previously. The result measured using a spectrum-impedance analyzer (Agilent 4396B) to which a reader antenna was connected (Figure 2.5(a)) shows the resonant dips observed in the antenna's impedance phase for three different conditions, i.e., before the expansion, after the partial expansion (to 4-mm diameter), and after the full expansion (to 6-mm diameter). As can be seen, the resonant frequency of the device shifted to lower levels as expansion progressed; this behaviour is anticipated, as the larger the radial cross-sectional area, the higher the inductance of the stent (that is a solenoid-like inductor), which lowers the resonant frequency of the device. The change of inductance was verified by establishing wire interface to the device at three different expansion conditions as summarized in Table 2.1, which shows steady raises of inductance with expansions whereas the capacitance and resistance were relatively stable in the expansion process. Small increases of the resistance with expansions seen in the table might be related to the strains applied to the stent structure upon expansions. (The increase in electrical resistivity of type-316L stainless steel due to tensile stress was reported [25]. It should be noted that the inductance rise also enhanced the inductive coupling between the device and antenna, resulting in larger phase dips with expansions (Figure 2.5(a)), as well as enlarging the Q factor of the device (Figure 2.5(b)). These results suggest that the RF power transfer to the device will be maximized when the device is fully deployed upon implantation, an ideal condition for the targeted application.

Device state	Inductance (nH)	Capacitance (pF)	Resistance (Ω)	Resonant frequency (MHz)
Unexpanded	191.0	2.95	13.6	205.3
Partially expanded	274.5	2.74	14.9	173.8
Fully expanded	387.5	2.86	17.4	147.6

Table 2.1: Values of electrical parameters measured with fabricated active stent at three different expansion conditions.

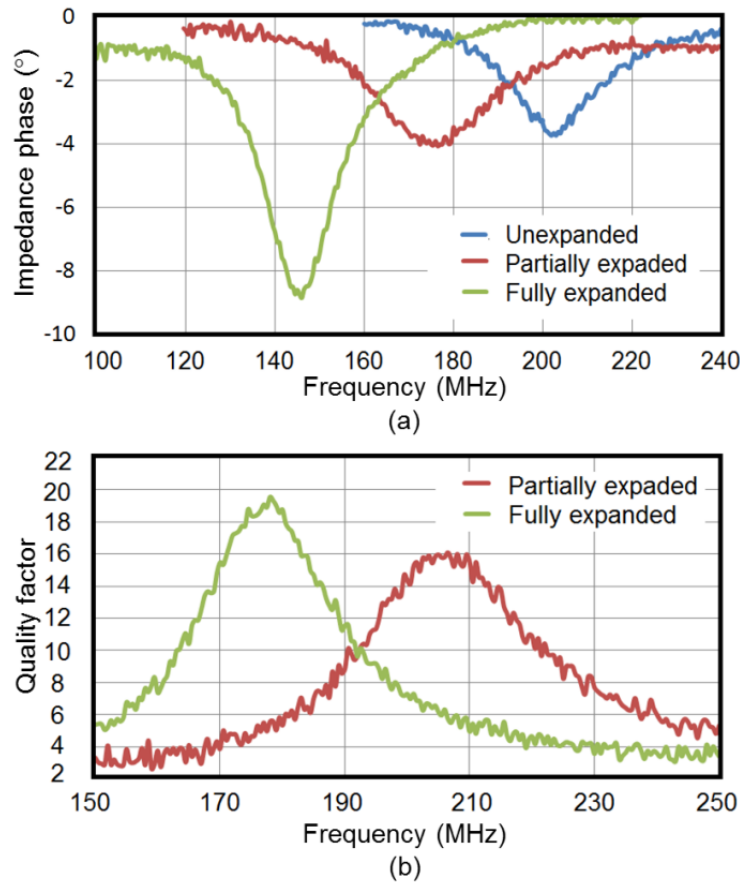


Figure 2.5: Measured device resonance frequencies and Q factors: (a) Resonant dips in impedance phase of reader antenna and (b) Q factors of the device at different expansion conditions measured as a function of frequency.

The EMF generated in the RF-excited stent (partially expanded state) was acquired using a digital oscilloscope that was wire interfaced to the stent. To observe the dependence of

power transfer on the frequency, the field frequency was scanned about the resonant frequency of the stent device (around 173 MHz) while using a constant RF output power of 320 mW fed to the transmission antenna. The stent device was positioned with respect to the antenna so that the axial direction of the stent was in parallel with the loop plane of the antenna. The EMF waveforms were recorded in the device (in close proximity to the antenna) that were excited at different field frequencies as shown in Figure 2.6(a), and the amplitudes of the waveforms as a function of the field frequency are plotted in Figure 2.6(b). As is clearly displayed, the EMF peaked (~900 mV) at the resonant frequency of the device, at which point the power transfer to the device for heat generation was maximized. The EMF amplitudes with varying distances between the antenna and the stent device were also characterized (Figure 2.6(c)) to show a strong dependence of EMF on the antenna-device separation up to ~3 mm at which the EMF reduced to 32% of the maximum level observed.

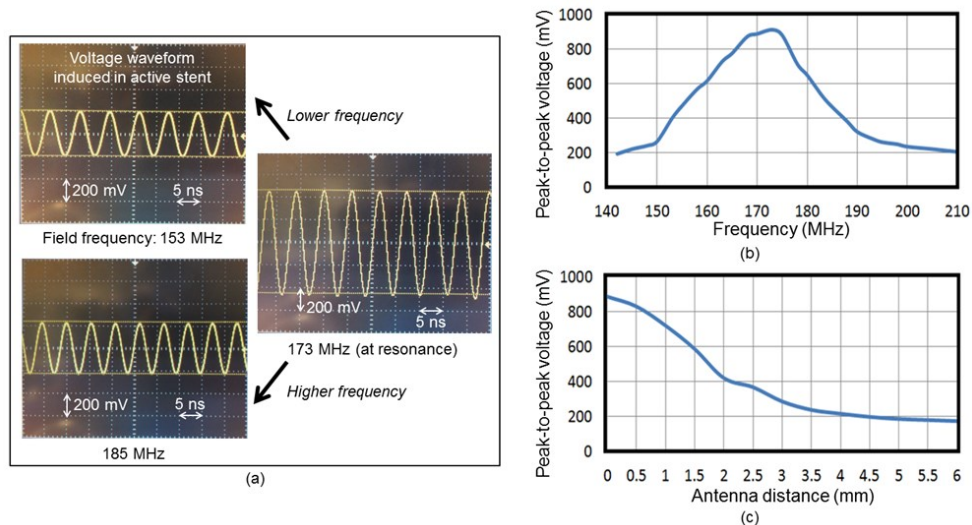


Figure 2.6: Device EMF measurement: (a) EMF waveforms generated in the partially expanded stent device due to RF excitation. (b) Measured EMF amplitude as a function of field frequency and (c) distance between antenna and device (at resonance).

2.3.3 Device RF heating tests

The experimental set-up used for wireless heating tests is shown in Figure 2.7. RF electromagnetic fields are generated using a loop antenna (diameter 1-2 cm) aligned to the tubular axis of the stent and connected to an RF signal generator (HP 8657A) through an amplifier. The device temperature is monitored and analyzed using an infrared (IR) camera (Junoptik VarioCam HiRes 1.2 M, Germany) and its custom software.

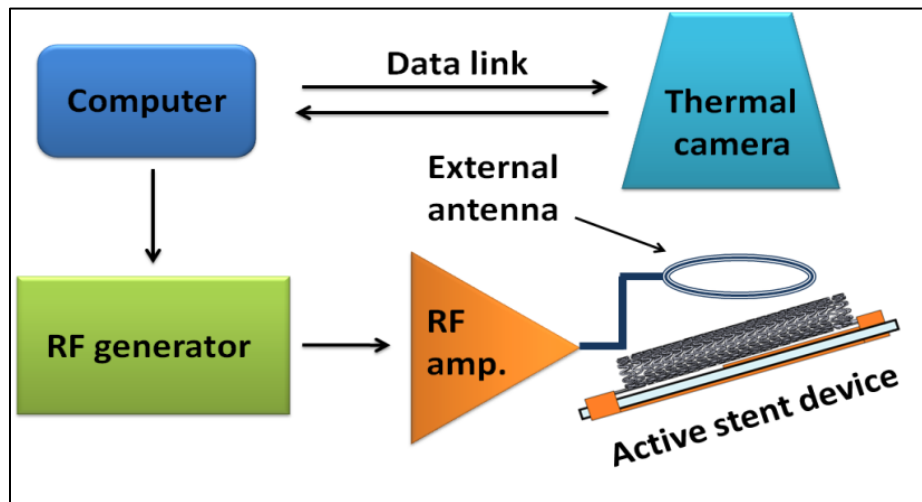


Figure 2.7: Experimental set-up used for wireless heating tests.

The RF heating test is conducted with two scenarios. Firstly, the stent device is placed through the RF antenna coil with central alignment in order to receive maximum RF energy transfer. Under this set-up, the stent device would be wirelessly heated up with a maximized inductive coupling and power transfer (as the direction of the produced magnetic flux matches the axis of the stent inductor). Secondly, the stent device is placed in parallel to the RF antenna coil and evaluated. This arrangement represents a more realistic scenario in terms of the actual use of the device in a clinical setting, where the antenna is placed on the skin of a patient to whom the stent device is implanted, while sacrificing the degree of inductive coupling between the antenna and the device.

compared with the former setting. In this case, RF signal degradation would be considered and the RF heating temperature of the device should vary with the distance between device and antenna.

Case 1: Device positioned through antenna loop

The temporal and frequency responses observed with the unexpanded device are displayed in Figure 2.8(a) and 2.8(b), respectively, and those of the same device fully expanded in the mock artery (with 6-mm diameter) are shown in Figure 2.8(c) and 2.8(d), respectively. Each result shows two temperature plots, one measured at the location where temperature peaked in the device and the other at an edge of the device (around the bonding terminal). IR images of the device before RF excitation and after the excitation are respectively shown in Figure 2.9(a) and 2.9(b) for the unexpanded device and Figure 2.9(c) and 2.9(d) for the fully expanded device. As indicated in Figure 2.9(b) and 2.9(d), the maximum temperatures were observed around the locations where the antenna loop was positioned (approximately the center of the stent); this is a reasonable outcome as the power transfer to the device is expected to be maximized at the locations closest to the antenna. As can be seen in Figure 2.8(a), the unexpanded device exhibited a rapid temperature rise upon the RF excitation, being heated up to 60 °C in 10 seconds, after which the device temperature slowly increased and saturated toward around 70 °C. Turning off the RF decreased the temperature quickly within ~ 5 seconds, followed by decelerated dissipation of heat. As indicated in Figure 2.8 as well as in Figure 2.9(b) and 2.9(d), the temperatures at the edges of the stent were substantially lower than that at the center of the device; this large thermal gradient appears as the edge regions are not part of the inductor and thus do not produce heat by themselves. i.e., temperature rise at those

locations is because of heat flux from the main (inductive) body of the stent device. The temporal response of the fully expanded device (Figure 2.8(c)) exhibited relative slow rise of temperature compared with the above case; this might be because, in contrast to the unexpanded device, the fully expanded one was surrounded by the artificial artery tube, i.e., heat dissipation to the tube might have slowed temperature increase. However, it should be noted that the device eventually reached temperature higher than that of the unexpanded case just before turning off the RF field (e.g. 75 °C on the surface of the artery tube vs. 70 °C on the device surface, at 40 seconds of excitation time); this outcome is likely due to the fact that the fully expanded device had a larger inductance compared with the unexpanded one, leading to a stronger inductive coupling with the antenna and more power transfer to the device. In terms of the frequency dependences of heating, comparing between the field frequencies where temperatures peaked in Figure 2.8(b) and 2.8(d) and the measured resonant frequencies of the device under unexpanded and fully expanded conditions (the latter had a smaller f_r level – refer to Table 2.1) clearly supports the theoretical condition that RF heating effect becomes the highest when the field frequency matches f_r of the LC -tank device. Another interesting observation in comparison between Figure 2.8(b) and 2.8(d) (showing temperature dependence on field frequency for the identical range of 100 MHz) is that the fully expanded device exhibited a narrower bandwidth in heat production compared with the unexpanded one; this is likely related to the fact that the former device had a higher Q factor than the latter.

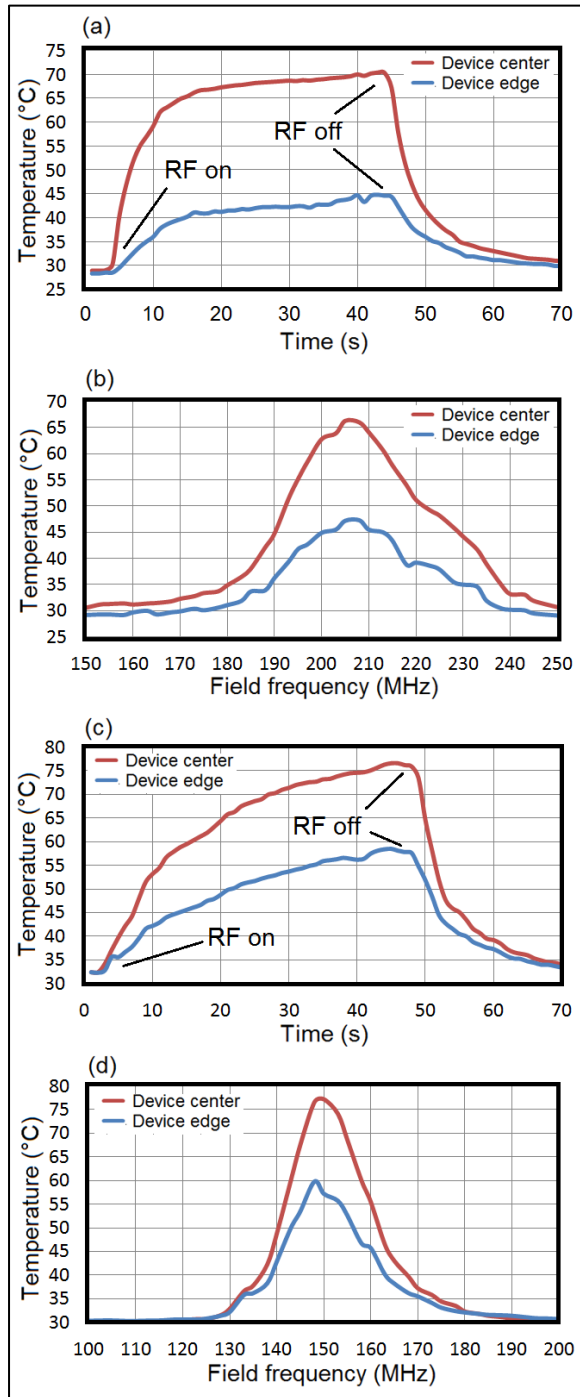


Figure 2.8: Measured thermal responses of stent device located through the antenna loop: (a) Temporal behaviour of stent temperatures (at the center and edge regions) with RF switching, and (b) generated temperature vs. field frequency observed in the unexpanded device, and (c)-(d) those observed in the fully expanded device inside the artificial artery.

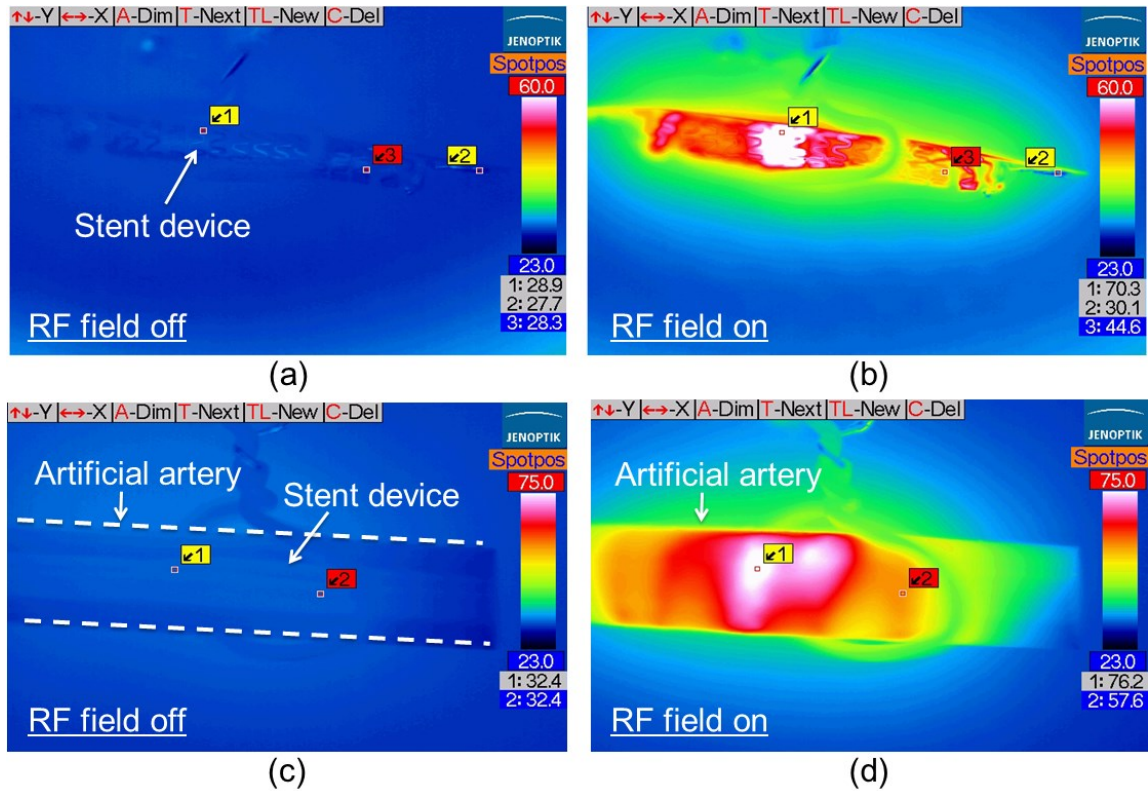


Figure 2.9: IR images of stent device located through the antenna loop before expansion: (a) without and (b) with RF excitation and the device fully expanded inside the artificial artery (c) without and (d) with the excitation implemented using the identical RF output power.

Case 2: Device positioned in parallel with antenna loop

The measurements were repeated under the other wireless setting, where the loop antenna was placed in parallel and proximity to the device for its excitation. The same set of measured data of temporal and frequency responses as well as IR images of the unexpanded and fully expanded device are shown in Figure 2.10 and 2.11, respectively. The maximum temperature in the unexpanded device was seen around the central region of the stent, reaching up to 57.7 °C (Figure 2.11(b)). A similar heating process was observed in the fully expanded device inside the artificial artery as well, with the maximum temperature of 63.8 °C on the surface of the artery tube, again around the

center region of the stent (Figure 2.11(d)). It can be seen from Figure 2.10(a) and 2.10(c) that the temperature rise observed in the expanded stent was substantially (22%) higher than that for the unexpanded case, which is most likely due to the predicted effect of enhanced power transfer. As can be seen in the time-domain measurement (Figure 2.10(a)), temperature of the stent rapidly increased as soon as the RF field was turned on, similar to the case of the previous antenna arrangement, providing the maximum temperature rise of 27 °C, in which 90% of it was completed in ~10 seconds. A tendency of somewhat slower response was seen with the fully expanded device in the artificial artery tube (Figure 2.10(c)); this supports its potential cause due to heat dissipation to the surrounding artery tube as discussed. The measured frequency dependences of heating (Figure 2.10(b) and 2.10(d)) indicate the temperature peaks at the field frequencies corresponding to the resonant frequencies of the two types of devices, along with a narrower active range with respect to the field frequency in case of the fully expanded one, both of which are consistent with the outcomes obtained in the other antenna arrangement. These results validate strong frequency selectivity in the operation of active stent even under the condition that the antenna and the device are arranged in parallel, a requirement toward real applications of the device and technology.

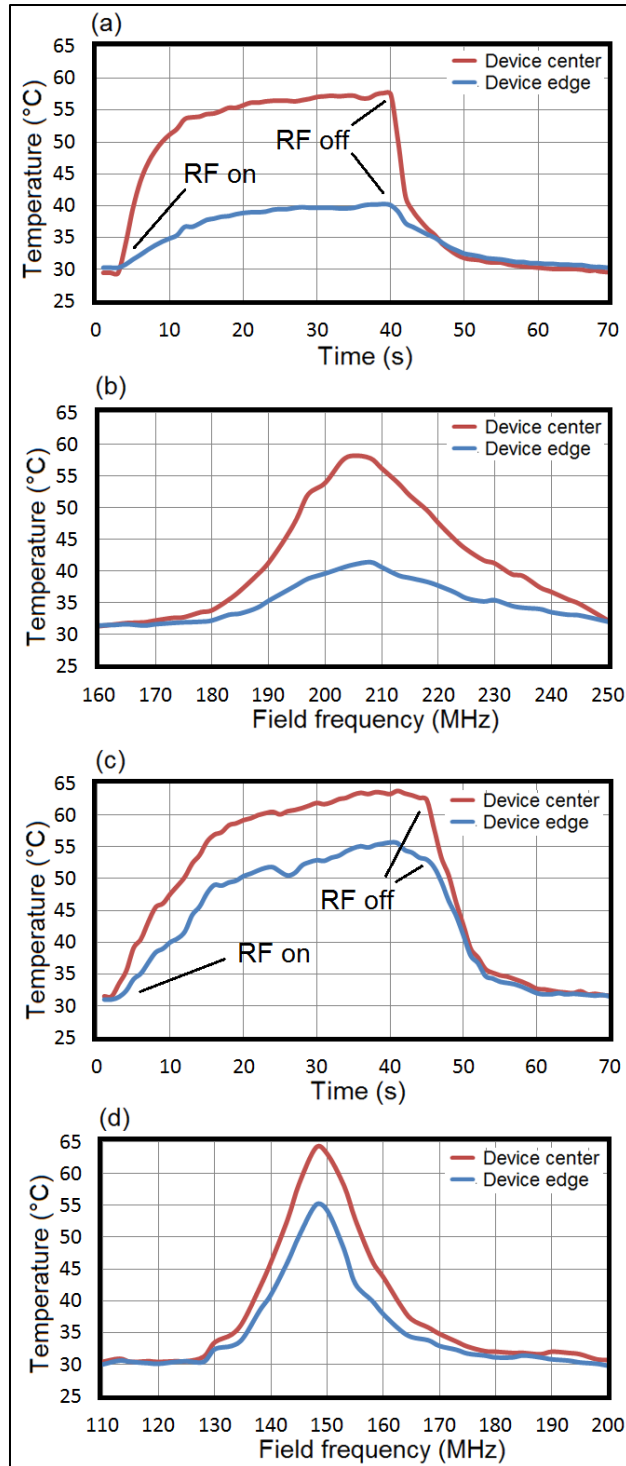


Figure 2.10: Measured thermal responses of stent device located in parallel with the antenna loop: (a) Temporal behaviour of stent temperatures (at the center and edge regions) with RF switching, and (b) generated temperature vs. field frequency observed in the unexpanded device, and (c)-(d) those observed in the fully expanded device inside the artificial artery.

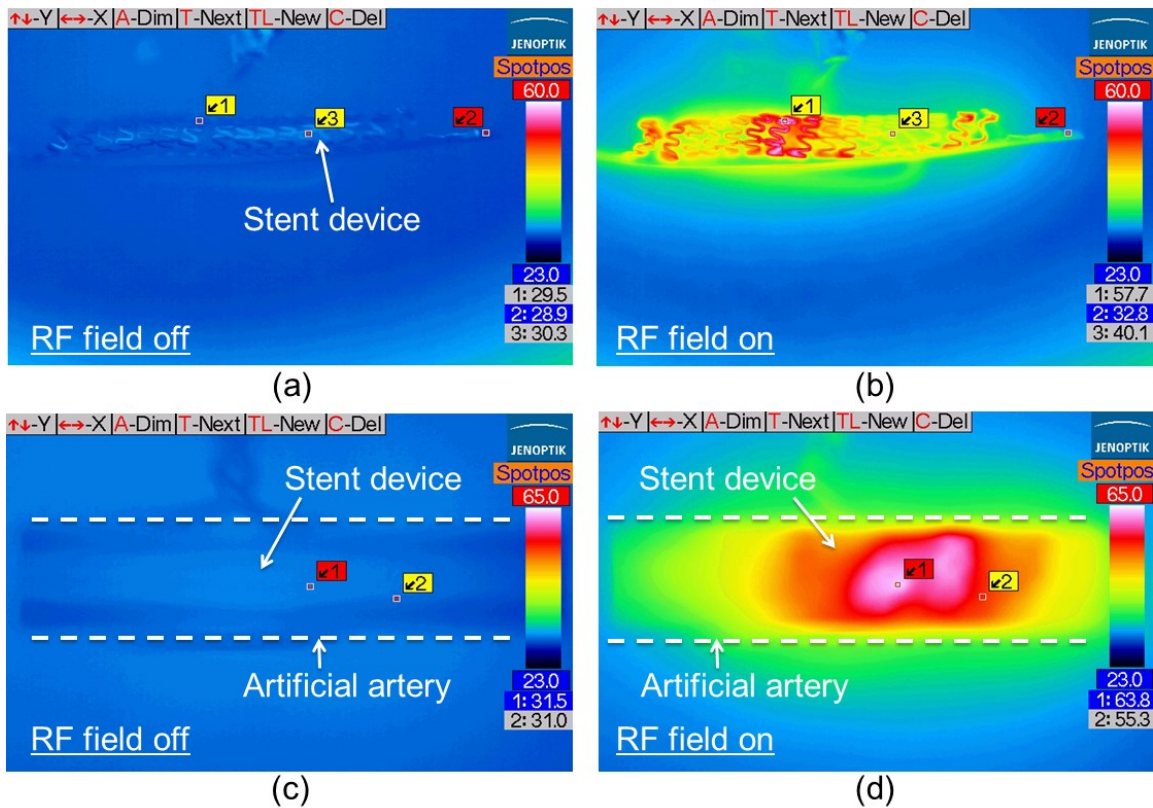


Figure 2.11: IR images of stent device located in parallel with the antenna loop before expansion: (a) without and (b) with RF excitation and the device fully expanded inside the artificial artery (c) without and (d) with the excitation made using the same RF output power.

As the field strength decays with distance, RF heating in the device should be substantially dependent on its distance from the transmission antenna. This effect was experimentally characterized. Figure 2.12 shows temperatures induced in the fully expanded device (using the same RF output power of 320 mW) with varying antenna distances in the parallel arrangement. The graph indicates that the temperature increase of 33 °C in the center of the device at the zero antenna distance dropped to 8 °C (the minimum target temperature rise) when the antenna was located ~3 mm away from the

device and that it diminished to zero as the distance reached ~6 mm with the device and set-up used in this test.

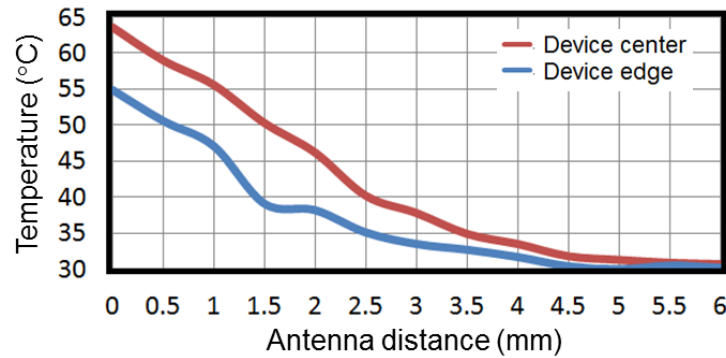


Figure 2.12: Generated temperature vs. device-antenna distance measured with the fully expanded device.

The initial experiments discussed above verified the effectiveness of the device concept and the functionality of fabricated prototypes with promising results, while revealing certain points that need to be investigated further toward clinical applications. The wireless tests showed that the device could produce heat with temperature rises greater than the target level when excited with a few millimeters of antenna-device distance. This wireless distance should be extended while maintaining RF radiation powers to a biologically safe radiation level [26]. One design strategy towards this direction may be to increase the efficiency of resonant heating, i.e., increase the Q factor of the stent device. This further suggests a reduction of the parasitic resistance of inductive stent (as also suggested in Eq. (2.1) or (2.2)), which is based on stainless steel that has a relatively high resistivity (for type 316L, it is, e.g., $\sim 44\times$ larger than that of Cu) and/or increasing the inductance of the stent (to maximize inductive coupling and power transfer). Although the latter may be approached by optimizing the three-dimensional helical

pattern of inductive stent, the former measure is more straightforward (as the latter involves simultaneous modification of mechanical performance as a stent) and proven to be effectively achieved by coating thin film of highly conductive metals (e.g. gold, which is also biocompatible) on the stent to exploit the skin effect [19]; metal coating is a promising path to improving thermal and wireless performance of the active resonant stent. Device packaging is another improvement aspect. The capacitive strip used to form the *LC*-tank on the stent is relatively large and may cause issues in stent crimping and delivery into blood vessels. Integration of capacitive components on the inductive stent is investigated as part of the circuit breaker development discussed in the next chapter.

Chapter 3

Biocompatible Circuit-breaker Chip for Thermal Management

As mentioned in previous chapters, the functionality of temperature regulation of the active stent device is enabled by using a thermal sensitive MEMS actuator. This chapter discusses a thermoresponsive micro circuit breaker researched for biomedical applications specifically targeting at intelligent electronic implants like active stents. The circuit breaker is micromachined to have a SMA cantilever actuator (discussed in section 3.1) as a normally closed temperature-sensitive switch to protect the device of interest from overheating, a critical safety feature for smart implants including those that are electrothermally driven with wireless micro heaters (Figure 3.1). The developed circuit-breaker chip (introduced in section 3.2) operates in a fully passive manner that removes the need for active sensor and circuitry to achieve temperature regulation in a target device, contributing to the miniaturization of biomedical microsystems including electronic smart implants where thermal management is essential.

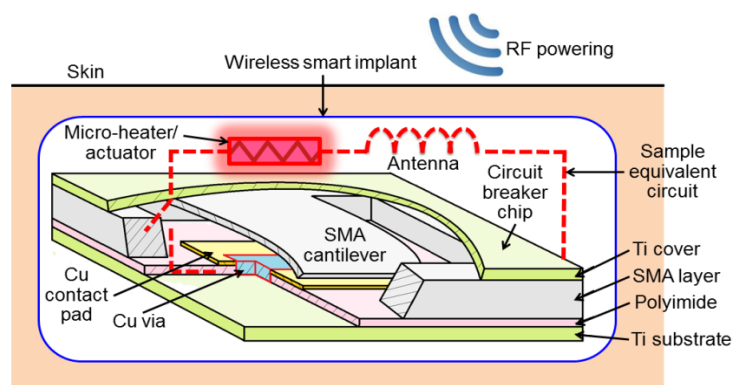


Figure 3.1: Conceptual illustration of the circuit-breaker chip and its application for temperature regulation of wireless “smart” implant such as implantable drug-delivery device driven by RF-powered micro heaters or electrothermal actuators.

3.1 Design of thermally sensitive MEMS actuator

The circuit breaker investigated is inserted into a power line of the circuit of interest in close proximity to the region that behaves as the main heat source so that produced heat is directly transferred to the breaker switch. When temperature in the switch rises to the SMA's threshold temperature, austenitic-phase temperature, the circuit breaker actuates to cut off the current path in the circuit until the temperature drops below the threshold. Large forces provided by SMA cantilever actuators [27] will be an advantageous feature to ensure breaking of the circuit even when stiction or micro-welding occurs at the contact [28]. The SMA actuator designed for the target circuit-breaker device is essentially a bimorph structure that is comprised of bulk-micromachined SMA cantilever coated with a thin-film reset layer. The cantilever of SMA is designed to have the flat state as the memorized shape, which is restored when temperature of the material is elevated to exceed the threshold level. At low temperatures (with which the SMA is in its martensitic phase), the material becomes compliant, and a mismatch in the coefficients of thermal expansion (CTE) between the SMA and the reset layer material is exploited to bend the cantilever down for its tip to make contact with the electrode pad created on the substrate, forming a normally-closed switch. In this study, thin-film SiO₂ is used as the reset layer to be formed on top of the SMA cantilever to generate a compressive stress, inducing the downward bending of the cantilever structure (Figure 3.2(a)). The vertical displacement of the free end of the SMA cantilever, d , can be expressed with the following relationship:

$$d = r - r \cos(\theta), \quad \cos(\theta) = \frac{r - d}{r} \quad (3.1)$$

where r and θ are the bending radius and angle, respectively, as shown in in Figure 3.2(b). The radius r can be expressed as [15]:

$$\frac{1}{r} = \frac{6W_1W_2E_1E_2t_1t_2(t_1+t_2)(\alpha_1-\alpha_2)\Delta T}{(W_1E_1t_1^2)^2 + (W_2E_2t_2^2)^2 + 2W_1W_2E_1E_2t_1t_2(2t_1^2 + 3t_1t_2 + 2t_2^2)} \quad (3.2)$$

where W , t , α , and E are the width, thickness, CTE, and Young's module of SMA (with subscription 1) and SiO₂ (with subscription 2), respectively, and ΔT is the temperature rise from room temperature. Equation (3.2) analytically suggests that the thicknesses of the two layers are important parameters that have major impacts on the level of bending among others.

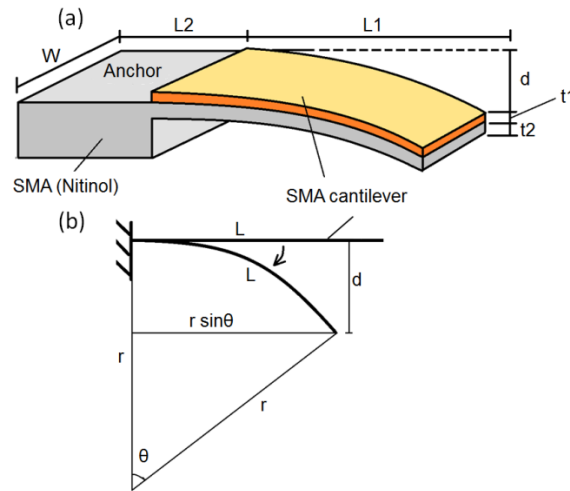


Figure 3.2: A cantilever model of the bimorph SMA actuator used for the circuit-breaker device showing (a) dimensional parameters of the structure and (b) other parameters relevant to the bent condition of the cantilever.

To design the Nitinol cantilever with a desired displacement at its cold state, the size of the cantilever and the thickness of the SiO₂ layer are determined through finite element analysis (FEA) using a COMSOL Multiphysics[®] software package (version 4.1). The cantilever is targeted to provide a cold-state displacement of 170-180 μm . Simulation

results suggest that the cantilever provides a total out-of-plane displacement of $174.3 \mu\text{m}$ at room temperature (Figure 3.3(b)) with a $4.0\text{-}\mu\text{m}$ -thick SiO_2 layer deposited under $250 \text{ }^\circ\text{C}$ on top of a $10\text{-}\mu\text{m}$ -thick, 1.5-mm -long Nitinol cantilever (Figure 3.3(a)). These values are utilized to develop the breaker device in this study.

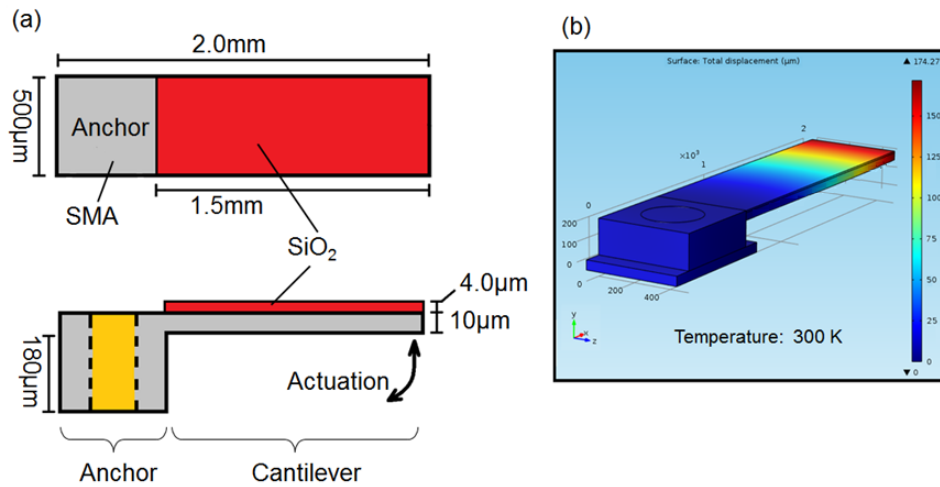


Figure 3.3: The proposed bimorph cantilever structure: (a) Design of Nitinol SMA cantilever actuator for the circuit breaker and (b) FEA simulation for displacement of the cantilever with SiO_2 reset layer indicating a downward free-end displacement of $174.3 \mu\text{m}$ at room temperature.

3.2 Chip based circuit breaker design

The active component of the circuit breaker is desired to be sealed within a chip-based frame for the device protection and the ease of integration with other circuits, just like many commercial MEMS products. The Nitinol actuator should be functional within and protected/isolated by a sealed chamber yet electrically connected to circuits outside. In addition, the packaging frame should be made of biocompatible materials to ensure medical safety of the chip when it is implanted into patient's body as part of a target smart implant, while providing high thermal conductivity to ensure efficient heat transfer to the Nitinol actuator inside of the chip for prompt triggering. Fulfilling those packaging

criteria is achieved with the device construction shown in Figure 3.1. Instead of using a small-footprint anchor (the case shown in Figure 3.3) being bonded on the substrate, the SMA cantilever is held by a rectangular-shaped frame of the same Nitinol that serves as one of the layers of the chip. This frame provides a platform for bonding with other layers and serves as the side walls of the chip. To form a contact switch, a Cu electrode pad is patterned on the central portion of a polyimide substrate layer on which the Nitinol layer is bonded. The tip of bent Nitinol cantilever touches on this pad to close the switch while the polyimide layer isolates the pad from the Nitinol layer. To support the polyimide layer and create an electrical connection from the Cu pad to outside, a rigid Ti plate with the same size as the chip is attached on the backside of the polyimide layer and electrically connected to the Cu pad through a via created in the layer, serving as an electrical terminal to be connected with an external circuit. A Ti cover is bonded on top of the Nitinol frame, sealing the cantilever inside. The top Ti layer serves as the other electrical terminal of the breaker. As represented by the equivalent circuit shown in Figure 3.1, the Nitinol actuator sealed inside shorts or opens these two terminals depending on the amount of heat applied to the chip.

In the nominal (cold) state, the SMA cantilever is at its bent condition to close the switch, allowing power supply to the external circuit that generates heat. Once heat flux coming from the circuit is high enough to trigger the actuation of SMA cantilever to return to its flat shape, the switch temporarily breaks the circuit to stop powering to the circuit and lower its temperature, preventing overheating. The chip may be directly mounted on a terminal of target circuit to connect the bottom or top pad of the chip to the circuit, and a wire could be bonded between the other pad of the chip and another terminal of the

circuit to insert the circuit breaker in series. The location of this chip should be arranged to be adjacent to the main heat source of the circuit, so that heat generated by the circuit quickly flows to the chip without substantial loss. For this purpose, direct mounting of the chip on the circuit may be performed using its top pad because this pad is directly bonded to the SMA layer in contrast to the bottom pad (where the polyimide layer is present between the pad and the SMA) so that heat transfer to the SMA cantilever is more efficient. The outer surfaces of the breaker chip consist of Ti, Nitinol, and polyimide that are all considered as biocompatible materials [29]–[32].

3.3 Chip fabrication

Although the circuit breaker chip has to be designed large enough to contain the SMA actuator, it still should be suitable for stent integration with a minimized overall device size. A chip with a smaller size lowers invasiveness to body after implantation, but it requires higher fabrication precision and alignment. Considering the trade-offs, the dimensions of the chip was determined as summarized in Table 3.2.

Chip length	2.0mm
Chip width	1.5mm
Titanium cap thickness	100 μ m
SMA actuator thickness	190 μ m
SMA cantilever size	0.5mmX1.5mm
Polyimide layer thickness	50 μ m
Cu clad layer thickness	5.0 μ m
Titanium layer/substrate thickness	100 μ m
Total chip thickness	450 μ m

Table 3.2: The specification of the circuit-breaker chip applied for fabrication.

The fabrication process of the circuit-breaker chip is shown in Figure 3.4. As discussed, there are three main layers to construct the designed circuit-breaker chip, i.e., the active Nitinol layer, the polyimide substrate with the bottom Ti pad, and the top Ti cover. The fabrication of the Nitinol layer (Figure 3.4, steps 1-3) starts from patterning of a cavity (1.1-mm wide, 1.7-mm long, and 180- μm deep) at the center of a 190- μm -thick Nitinol plate (Alloy M, Memry, Germany; austenitic start temperature (A_s) = 56.5 $^\circ\text{C}$, martensitic start temperature (M_s) = 53.5 $^\circ\text{C}$) with the size of 2.0 \times 1.5 mm² using micro-electro-discharge machining (μEDM ; EM203, SmalTec International, IL, USA). This cavity defines the thickness of the Nitinol cantilever. The shape of Nitinol cantilever is further patterned with μEDM by cutting through the bottom layer of the cavity, creating spaces between all sides of the cantilever and the outer frame the Nitinol plate. Next, a 4.0- μm -thick SiO_2 reset layer is deposited on top of the Nitinol cantilever (backside of the cavity region) using plasma-enhanced chemical vapor deposition at 250 $^\circ\text{C}$. (After this step, the cantilever is bent due to a compressive stress induced by the SiO_2 layer as noted previously.) Then, a 200-nm-thick Cu layer (together with a 15-nm-thick Cr adhesion layer) is deposited on the backside of the cantilever using electron-beam evaporation. The fabrication of the substrate component (Figure 3.4, steps 4-6) uses a single-sided Cu-clad PI film with 50- μm thickness, prepared to have the size of the circuit-breaker chip. The 5- μm -thick Cu-clad layer is lithographically patterned in the center using dry-film photoresist (PM240, DuPont, DE, USA). Then the PI film is etched using KOH-based solution [24] to create a via hole (500- μm square) in the center. With the polyimide film aligned to a 100- μm -thick Ti plate (μEDM ed to have the same size as the chip), Cu

electroplating is performed in a sulphuric acid based bath to fill up the via hole and elect-

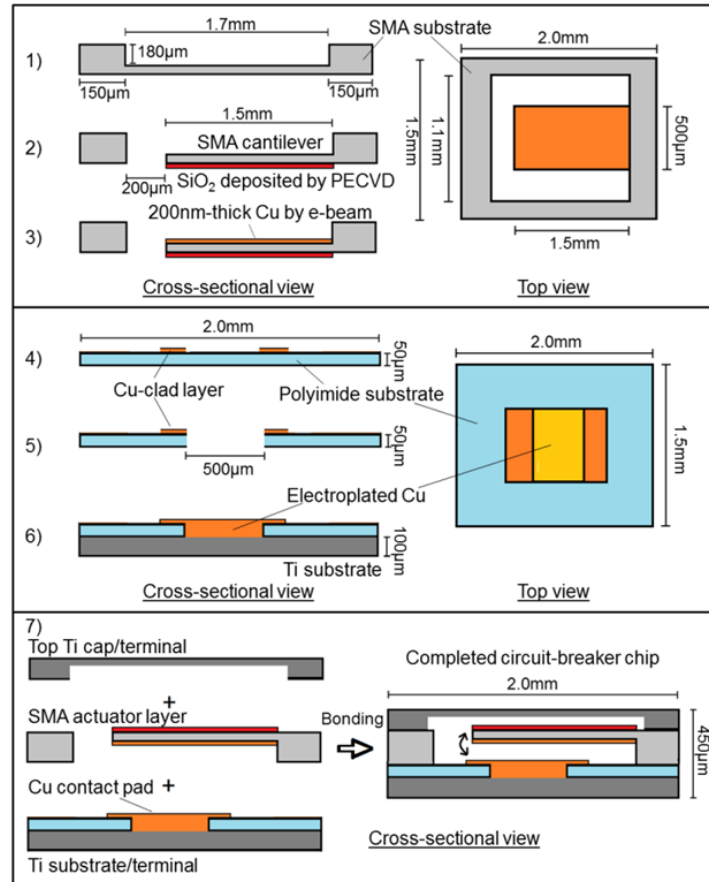


Figure 3.4: Developed process for the fabrication of the circuit-breaker chip.

rically connect the Ti plate to the patterned Cu clad layer, defining the final form of the contact pad for the cantilever switch on the substrate. The top Ti cap is shaped in a similar manner as the other (bottom) Ti plate, except for creating a 50-µm-deep cavity in the center to avoid potential contact of the cantilever with the bottom of the cap when combined. Finally, the circuit-breaker chip is assembled by bonding the Ti cap, the SMA actuator layer, and the bottom Ti plate together using conductive epoxy with precise alignment while applying a force (of 10 N) to the combination (Figure 3.4, step 7). A sample of the fabricated chip is shown in Figure 3.5(a). Scanning electron microscope (SEM) images of the Nitinol cantilever switch (Figure 3.5 (b) and 3.5(c)) indicate that at

room temperature, the tip of the cantilever touches down on the Cu electrode pad underneath as desired. The final thickness of the completed circuit-breaker chip is measured to be 460 μm (suggesting an average bonding layer thickness of 15 μm).

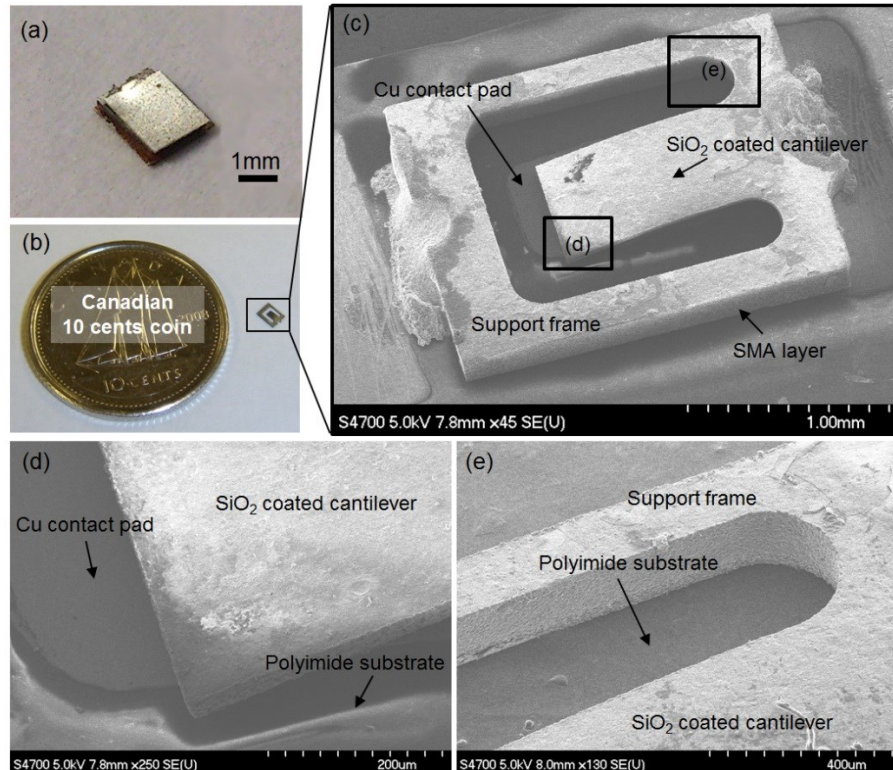


Figure 3.5: Fabrication results: (a) Completed circuit-breaker chip; (b) Nitinol actuator component patterned using μEDM ; SEM images of (c) Nitinol switch and (d)-(e) close-ups of the switch structure (locations indicated in Figure 3.5(c)).

3.4 Device characterization

Characterization results for the fabricated Nitinol actuator and circuit-breaker chip are presented in this section. Their performance with respect to the electrical and temporal responses is experimentally evaluated. In addition, experimental demonstration of wireless temperature regulation enabled with the fabricated breaker chip is presented and discussed.

3.4.1 Thermomechanical characteristics of the Nitinol actuator

The mechanical response of the Nitinol cantilever to thermal stimulation was first evaluated by increasing the temperature of the component (before packaging, up to ~ 80 °C) on a hot plate while measuring out-of-plane displacements of the cantilever using a laser displacement sensor (LK-G32, Keyence, ON, Canada; 10-nm sensing resolution) which laser spot was aligned at the free end of the cantilever. The temperature of the cantilever during this test was monitored and recorded using the IR camera that was located above the component and analyzed with the custom software. Figure 3.6 shows a typical measurement result of the cantilever's temperature (around the free end) and displacement tracked simultaneously with time. As shown, the Nitinol cantilever remained almost stationary until reaching ~ 58 °C (at ~ 25 seconds), after which the cantilever displaced upward and returned to its flat shape, leading to an approximate displacement of 220 μm when temperature reached ~ 66 °C (at ~ 35 seconds). These characteristic temperatures measured match well with the corresponding transitional temperatures (A_s of 56.5 °C and austenitic peak temperature (A_p) of 68.5 °C) of the Nitinol material used for this actuator.

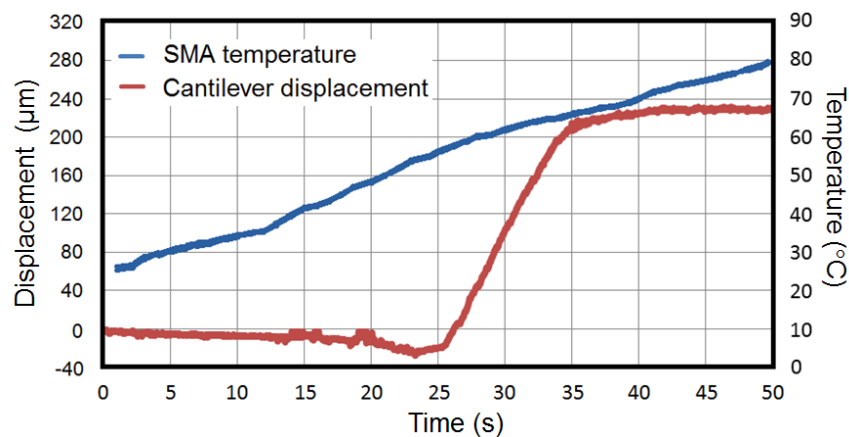


Figure 3.6: Measured temporal behaviour of free-end displacement of the Nitinol cantilever with temperature increase applied to the cantilever.

3.4.2 Electrothermal characteristics of circuit-breaker chip

The fabricated circuit breaker was characterized and tested using both the Nitinol switch itself (before bonding the Ti plates on both sides) and the completed chip (with the Ti plates bonded). Either device was heated using the hot plate while recording the electrical resistance between the two terminals of the device (the Cu contact pad and the bonded part of the Nitinol cantilever for the former device, and the top and bottom Ti plates of the chip for the latter case) as well as the device temperature using the IR camera. Measurement results shown in Figure 3.7 illustrate the electrical behaviour of each device as a function of temperature in a cycle of heating and cooling. As can be seen in Figure 3.7(a), the self-resistance of the Nitinol switch was measured to be approximately $10\ \Omega$ at room temperature. This base resistance stably remained until the device temperature rose to $\sim 55^\circ\text{C}$, at which the resistance showed gradual increases, followed by a rapid rise to infinity that represents the complete open state of the switch as the temperature passed around 63°C . As the switch cooled down, the resistance remained at infinite until the temperature decreased to $\sim 53^\circ\text{C}$, after which the self-resistance dropped rapidly and back to its initial state at $\sim 45^\circ\text{C}$. The observed hysteresis of the switch's behaviour is caused by that of Nitinol's phase transition; the corresponding threshold temperatures that characterize the hysteresis match well with A_s and M_s of the Nitinol material used. The measurement result of the packaged chip shown in Figure 3.7(b) indicates a hysteretic behaviour similar to that of Nitinol switch itself (Figure 3.7(a)). The self-resistance of the chip at low temperatures remained at around $14\ \Omega$, slightly larger than the previous case presumably due to an additional resistance involved in the Ti packaging of the switch.

Because of the self-resistance, the circuit-breaker chip may produce heat by itself when a current passes through the chip after being integrated into an external circuit. Knowing this self-heating effect is important in determining the device design as it defines the maximum current allowance for the circuit-breaker chip as well as the actual temperature of the external circuit that triggers the breaker chip. Figure 3.8 shows the measurement results that illustrate the self-heating effect induced in two scenarios - when the current passes through the chip is in a form of DC (Figure 3.8(a)) and that of RF (Figure 3.8(b)). For the DC case, the switch temperature was recorded (using a chip without the top Ti plate) as a function of the current amount. For the RF case, the same was performed as a function of frequency (up to 50 MHz) with varying signal amplitudes (0.5, 1.0, and 1.5 V) tested using a combination of an RF signal generator (HP8657A) and a power amplifier. As can be seen in Figure 3.8(a), the switch exhibited gradual temperature increases with the DC current; as the current rose to ~ 0.5 A, temperature reached $\sim 55^\circ\text{C}$, approximately the threshold temperature that opened the switch (Figure 3.7(b)). Therefore, the maximum DC current permitted for the fabricated chip should be less than 0.5 A. In the case of RF (Figure 3.8(b)), there were clear increases in breaker temperature

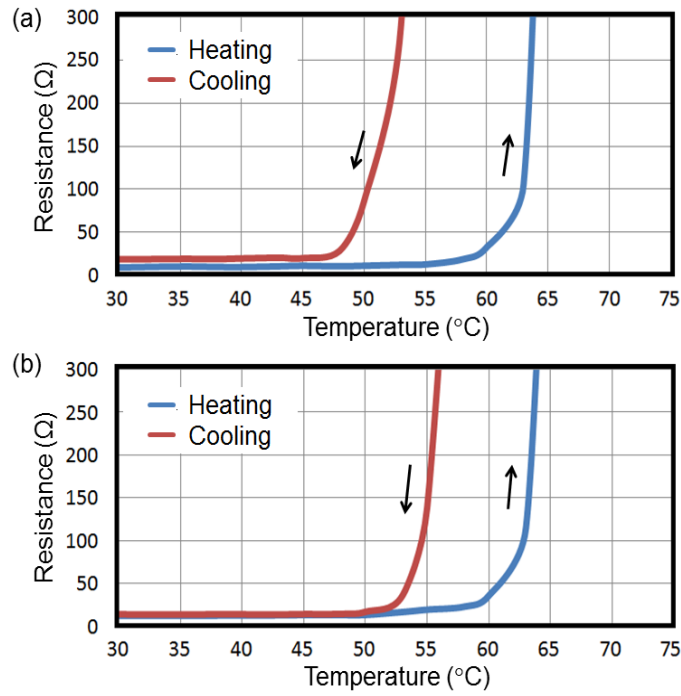


Figure 3.7: Electrical contact resistances of (a) standalone fabricated breaker switch (without Ti packaging) and (b) completed circuit-breaker chip (with Ti packaging) recorded as a function of temperature in a cycle of heating and cooling.

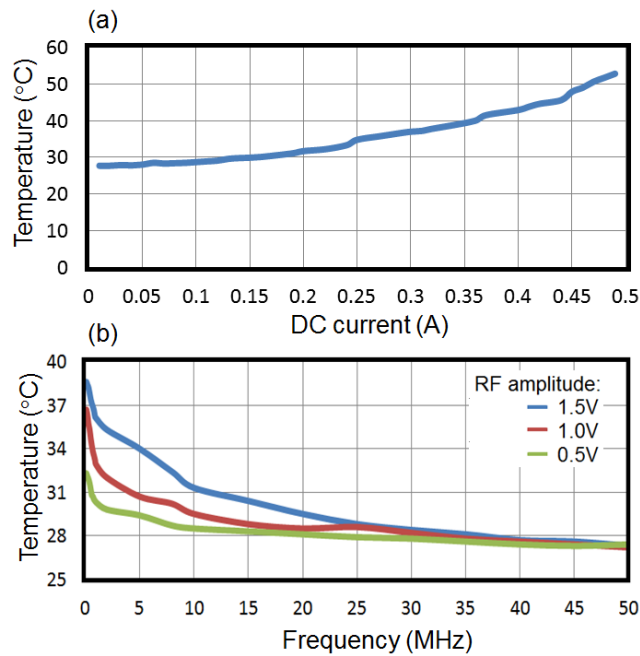


Figure 3.8: Self-heating effects of fabricated circuit-breaker chip observed by application of (a) DC and (b) RF signals fed to the chip.

with signal amplitude at low frequencies; however, this heating effect diminished towards nearly zero for all amplitudes as the frequency approached to 50 MHz. This situation in turn means that the triggering of the breaker may be solely determined by the external heat source under the frequencies over 50 MHz, which represents an ideal application area for the breaker device as the degree of self-heating could vary depending on the operation condition of the external circuit.

3.4.3 A preliminary application test: Temperature regulation of wireless resonant heater

One of the potential applications of the proposed circuit breaker is the temperature regulation of wireless heaters that have been utilized to enable active functions of different types of smart implants [16], [18]. These wireless heaters are essentially *LC* resonant tanks; radiation of an RF electromagnetic field results in inductive heating when the field frequency matches the resonant frequency of the tank [27]. This resonant heating principle has been adopted to enable controlled drug delivery from an implantable device using thermoresponsive active valves operated with the wireless heater [16] as well as the active stent [18] discussed in chapter 2. After implantation, these devices are operated by applying the field through the skin using an external transmission antenna placed on the skin. An apparent challenge in their operations is that depending on the location of the implant (that could involve varying thickness of tissue between the device and the skin where the field passes through, with different types of tissue (fat, muscle, bone, etc.) that exhibit different RF attenuation levels), the intensity of arrival field at the location of the implant varies. If the field intensity happens to become high under a certain condition, it could lead to a hazardous situation of overheating. The integration of the circuit breaker

with the wireless heater is expected to physically limit and automatically regulate inductive heating “on site” in any kind of unexpected circumstance, ensuring that the implant device works safely and reliably. This functionality allows the system to be operated in an open-loop and passive manner to achieve thermal regulation, simplifying the implant and system architecture. Having this application focus, the temperature regulation of RF resonant heating was studied using an experimental set-up shown in Figure 3.9. A test *LC*-tank heater coupled with a fabricated circuit-breaker chip (formed by series connecting a 420-nH solenoid coil, a discrete 10-pF capacitor, and the chip) was wirelessly excited with an RF field generated using an external coil antenna that was inductively coupled with the *LC*-tank. The external antenna was powered with the same RF signal generator-amplifier described earlier. The heater was activated by tuning the frequency of the generator, or that of the RF field, to the resonant frequency of the circuit (61 MHz) with an RF output power of 320 mW. Prior to this test, the resonance frequency of the circuit was precisely determined though the same inductive coupling using the same antenna (as a receiver antenna) connected with a spectrum-impedance analyzer (Agilent 4396B). The temperatures of both the wireless heater (inductor of the circuit) and the breaker chip coupled adjacent to it were simultaneously monitored and analyzed through the IR camera.

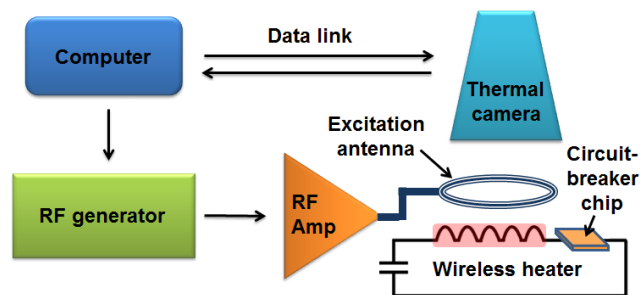


Figure 3.9: Experimental set-up used for wireless heating tests with an RF resonant heater.

The anticipated behaviour of this wireless system is as follows: With a tuned RF excitation, an EMF is generated in the circuit as it resonates, causing an RF current that generates heat in the inductor of the circuit. This heat is transferred to the circuit-breaker chip connected with the inductor to raise chip temperature, and, when it exceeds the designed threshold level, the chip opens the circuit to terminate the current and heating in the inductor, leading to heat dissipation and cooling of the inductor. The breaker closes the circuit again when its temperature becomes low enough, permitting the flow of induced current and resultant heating again. With continuous RF radiation, this open-close cycle of the breaker is self-sustained to regulate inductor's temperature within the threshold level defined by the breaker. Therefore, the circuit-breaker chip functions as an absolute temperature limiter for the devices that are operated with this type of wireless heaters. The measurement result shown in Figure 3.10 validates the designed function of the circuit breaker described above. As RF heating was initiated and the circuit breaker was heated up to ~ 63 °C, the Nitinol cantilever actuated to open the circuit. This actuation terminated the RF heating of the inductor, lowering temperature of the breaker down to ~ 51 °C, at which the breaker closed the circuit that restored the resonance to cause RF heating and temperature increase again. Overall, temperature of the wireless heater was limited below 55 °C while the breaker exhibited an oscillated temperature cycle between 51 °C and 63 °C. The breaker's role as a temperature limiter is evident from a comparison with the case that removed the breaker chip from the wireless heater excited under the identical condition, which led to the inductor temperature reaching over 90 °C as also shown in Figure 3.10. Therefore, this test experimentally proves that the microfabricated circuit-breaker chip is highly effective in regulating temperature of the

LC-tank-based smart implants within a desired range defined by the breaker.

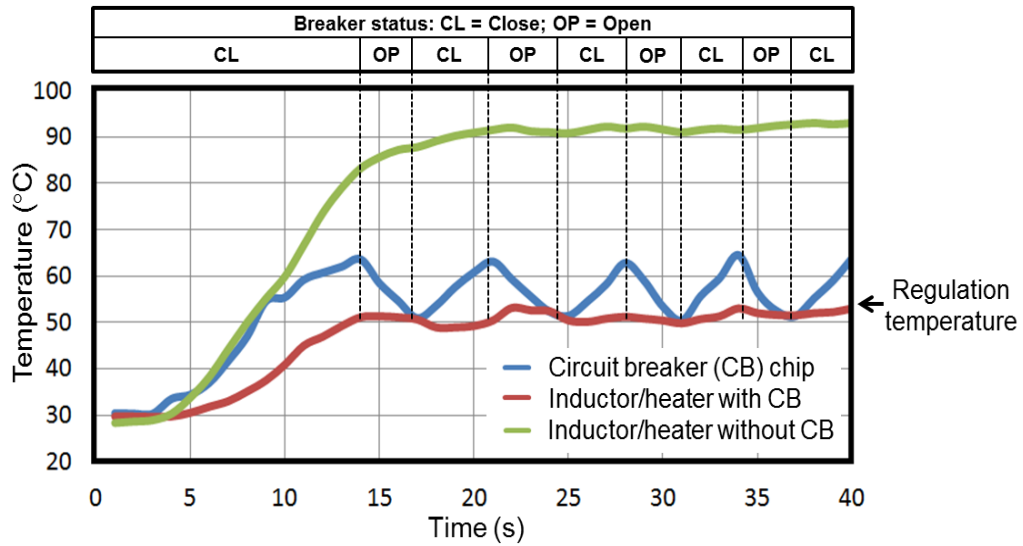


Figure 3.10: Measured thermal response of the circuit-breaker-coupled wireless heater showing self-regulated on-off cycle of the breaker chip and resultant temperature regulation observed in the heating inductor. The behaviour of the heater without the circuit breaker is also plotted for comparison.

Chapter 4

Active Stent with Temperature Regulation

In this chapter, the inductive stent is integrated with a capacitor-embedded circuit-breaker chip to demonstrate RF heating regulation in the active stent. The integrated stent device is expanded up to 6 mm in diameter inside an artificial artery using a balloon catheter. When RF excited, the expanded device is revealed to generate heat with temperature rise and bounce within a certain range managed by circuit-breaker chip. Temporal and frequency characteristics are evaluated to illustrate strong frequency sensitivity and regulated heating. *In-vitro* testing in liquid environment is also performed and discussed.

4.1 Working principle and device design

Same as the wireless stent device introduced in previous chapters, the resonant RF heating function is enabled by electromechanically coupling an inductive stent [19] described in chapter 2 with a capacitive element to establish an *LC*-tank circuit. The feature of temperature regulation is provided by the integration of the circuit-breaker chip described in chapter 3 on the stent device. As the chip temperature is modified by heat generated by the inductive stent, the breaker chip integrated on it implements reversible breaking of the *LC*-tank in the device to prevent it from overheating. When temperature of the breaker rises to the SMA's threshold level, austenitic-phase temperature, the circuit breaker actuates to cut off the current path in the tank until the temperature drops below the threshold. The design of the breaker chip is modified to incorporate a capacitive element to eliminate the capacitive strip from the device discussed in chapter 2.

The Nitinol layer that contains the actuator and a parallel-plate capacitor are coupled in series and titanium packaged together in the form of a $2.0 \times 1.5\text{-mm}^2$ chip as shown in Figure 4.1. The design of the circuit breaker used in this study is similar to the one discussed in the preceding chapter, except that a parallel-plate capacitor is combined with the chip. The capacitor structure is comprised of $50\text{-}\mu\text{m}$ -thick PI film, serving as the dielectric layer, sandwiched by titanium electrodes with the same size as the breaker chip, and provides a capacitance of 3.2 pF . This capacitive component is coupled with the backside of the breaker's polyimide substrate, which has a via that electrically connects the switch's contact electrode to one of the capacitive electrodes. The other capacitive electrode is used as one of the external terminals of the chip. The other side of the Nitinol layer is sealed by another titanium layer to encapsulate the cantilever switch, which serves as the other external terminal of the chip same as before. The top and bottom titanium terminals of the chip, therefore, provide electrical access to the series-connected MEMS switch and the capacitor element. One side of the chip is electromechanically bonded on one end of the inductive stent created to have a tab-like platform/terminal at each end for integration of the chip, and the other side of the chip is wire bonded to the other side of the stent's end tab to complete the circuit.

With a tuned RF excitation, an EMF is generated in the *LC*-tank stent as it resonates, causing an RF current that generates heat in the inductive stent. This heat is transferred to the circuit-breaker chip to raise its temperature, and, when the temperature exceeds the designed threshold level, the chip temporarily opens the circuit to terminate the current and heating in the stent, followed by cooling of the device. The breaker closes the circuit again when its temperature becomes low enough, permitting the flow of induced current

and resultant heating again. With continuous RF radiation, this open-close cycle of the breaker is self-sustained to regulate the stent's temperature within the threshold level defined by the breaker. Therefore, the breaker chip functions as a safety temperature limiter for the active stent. The chip is a standalone passive component that removes the need for any other component or separate power source with the implant for performing thermal management in the process of endohyperthermia therapy.

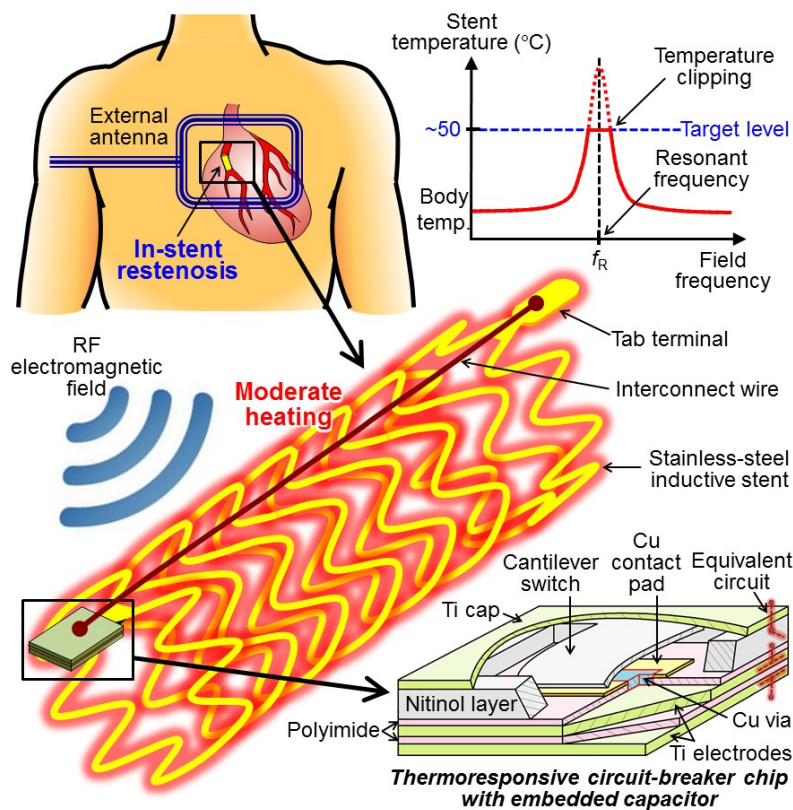


Figure 4.1: Endohyperthermia treatment of in-stent restenosis through the active LC-tank stent with the integrated MEMS circuit breaker that serves as a wireless heater with an absolute temperature limiter. Once implanted, the device is activated by resonating it using an externally applied RF electromagnetic field to perform the thermal therapy.

4.2 Fabrication

The fabrication process developed for a proof-of-concept prototype is illustrated in Figure 4.2. The detailed steps for the breaker fabrication are already provided in the preceding chapter. To add the capacitor to the chip, a piece of 50- μm -thick PI and that of 100- μm -thick titanium substrate with the size of the chip are prepared and bonded together with other layers in a similar manner to complete the chip, forming a series connected circuit breaker and parallel-plate capacitor (Figure 4.2, step-1).

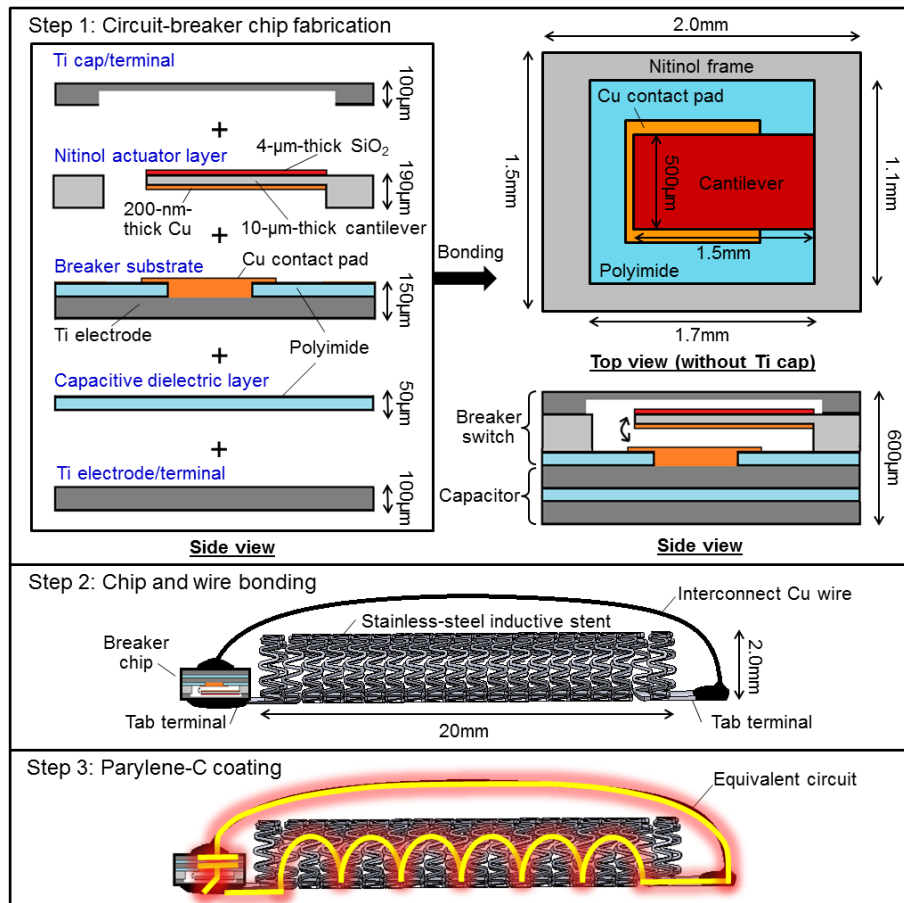


Figure 4.2: Fabrication process developed for the active stent device with the circuit-breaker chip.

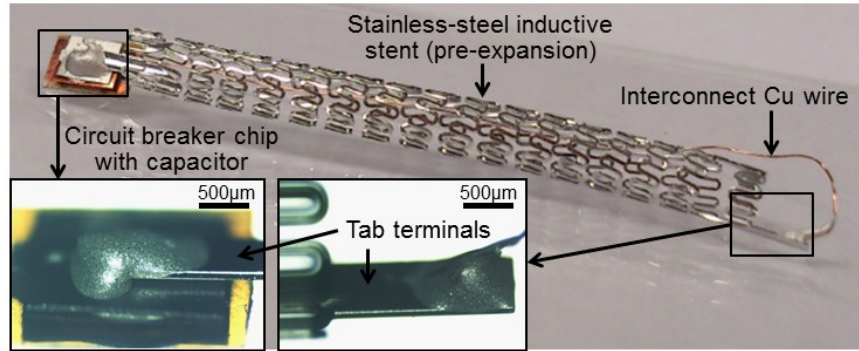


Figure 4.3: Fabricated active stent device (top) with close-up views of the integrated circuit-breaker chip (left) and the other side of the stent terminal on which the interconnect wire was bonded (right).

As noted earlier, the stainless-steel inductive stent is micromachined to have a tab terminal (with an approximate size of $1500 \times 500 \mu\text{m}^2$) at each end of the tubular body with an outer diameter of 2.0 mm [19] (Figure 4.3). To electromechanically couple the fabricated breaker-capacitor chip with this inductive stent, the Nitinol side of the chip is bonded to one of the end tabs of the stent using the conductive epoxy, and then the other terminal of the chip is electrically connected to the other end tab of the stent by bonding a Cu wire (80 μm thickness) between them; this completes the *LC* circuit, a combination of the stent and the on-chip capacitor, with the circuit breaker connected in series (Figure 4.2, step-2). The length of the interconnecting wire was arranged to be large enough to avoid a tensile force being applied to the wire (that could lead to failures of bonded terminals) during balloon expansion of the device up to 6 mm in diameter. The entire device assembly is finally coated with Parylene C for 4- μm thickness so that all the surfaces of the device are electrically and biologically insulated from surroundings (Figure 4.2, step-3). Figure 4.3 shows a sample of the completed device.

4.3 Experimental results and discussion

4.3.1 Device expansion

The radial expansion of the fabricated stent device was tested (after electrical characterization of the unexpanded device discussed later) using commercial angioplasty balloon catheters. To evaluate the device response with different expansion conditions, same as before, the catheters with two different balloon diameters (4.0 mm and 6.0 mm) were used. The prototype was first expanded partially from the initial 2.0 mm to 4.0 mm in diameter using the 4.0-mm balloon catheter on which the unexpanded stent device was mounted (Figure 4.4(a)), followed by deflating and retrieving the balloon from the device. After characterizing this partially expanded device, it was remounted on a deflated 6-mm balloon catheter and was further expanded by inflating the balloon inside the artificial artery with 6 mm in diameter (Figure 4.4(b)). In each expansion, the pressure of the balloon was increased to 12-15 atm by injecting water into it using a commercial inflator (Figure 4.4(a)), deforming the solenoid-like stent inductor along the cylindrical shape of the balloon. The fully deployed device in the artificial artery (after retrieving the balloon) is shown in Figure 4.4(c). No electrical or mechanical failures due to these expansions were detected in the prototypes tested in this study.

4.3.2 Electromechanical characterization

Having a solenoid-like geometry, the inductance and resultant f_r of the stent device vary as the device changes its geometry with balloon expansion. The larger the radial cross-sectional area, the higher the inductance of the stent (and thus lower the f_r). This dependence was first characterized while expanding the device in a manner described in

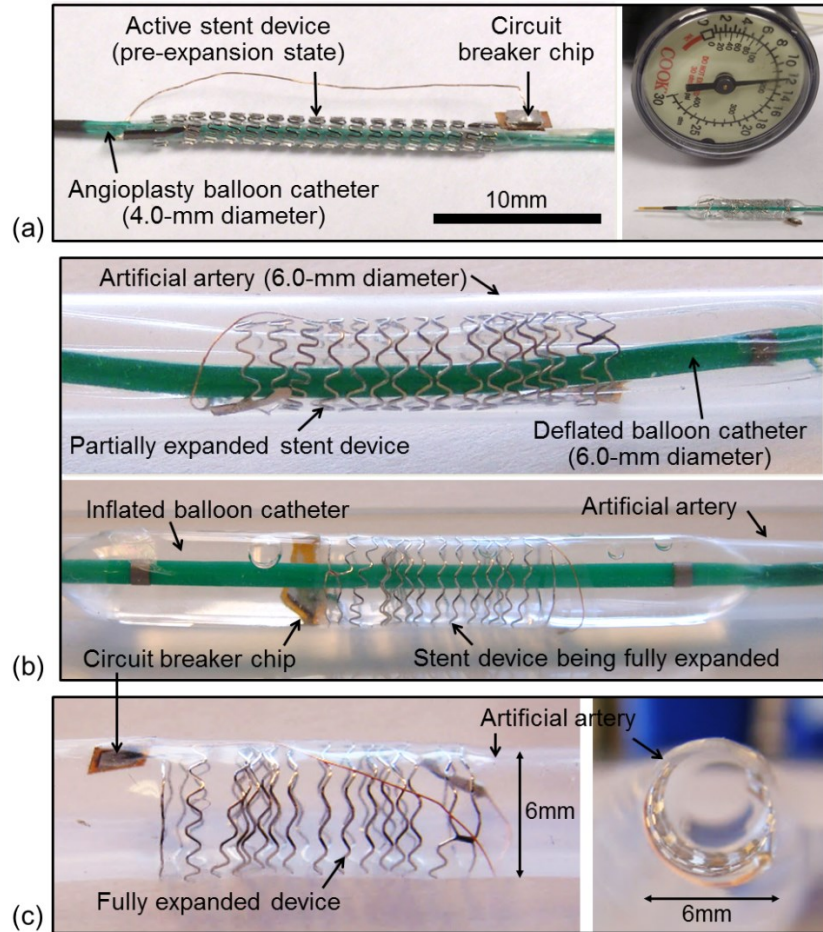


Figure 4.4: Expansion test results: (a) Fabricated device mounted on a deflated 4-mm balloon catheter before expansion (left) and after expansion by inflating the balloon at 12 atm (as shown in the pressure meter of the inflator) (right); (b) the partly expanded device mounted on a deflated 6-mm balloon catheter and positioned inside artificial artery with 6-mm diameter (top) and expanded by balloon inflation (bottom); (c) side (left) and axial (right) views of the stent device fully expanded within the artificial artery.

chapter 2 for three different conditions, i.e., before the expansion, after the partial expansion (to 4.0-mm diameter), and after the full expansion (to 6.0-mm diameter). Table 4.1 summarizes the inductance of the device along with its parasitic resistance at the three conditions, measured by establishing wire interface to the device (probing at left and right terminals of the device), showing consistent rises of the inductance as anticipated. It can

be seen that the stent provided an approximately $3\times$ larger inductance when fully expanded compared with the unexpanded case. It also shows that the resistance was relatively stable while exhibiting small increases with expansions; this slight variation was also observed in the previous result (chapter 2). The variation of the device's f_r was wirelessly probed by establishing an inductive coupling between the stent and an external loop antenna. The result measured using a spectrum-impedance analyzer (Agilent 4396B), which the reader antenna was connected (Figure 4.5(a)), shows the phase dips observed in the antenna's impedance that represents the resonances of the device corresponding to the three device conditions. The recorded shifts of the resonant frequency with expansion prove the anticipated frequency response of the device. It can also be seen that the inductance rise with device expansion enhanced the inductive coupling between the device and the antenna, leading to larger phase dips as the device was expanded. A similar effect by the inductance increase was also observed in the quality factor (Q factor) of the device (Figure 4.5(b)). These outcomes are consistent with the results obtained with the active stent discussed in chapter 2 (with capacitor strip and without the circuit-breaker chip).

Device state	Inductance (nH)	Resistance (Ω)	Resonant frequency, f_r (MHz)
Unexpanded	130	17.4	274
Partially expanded	228	18.3	195
Fully expanded	382	19.6	126

Table 4.1: Values of electrical parameters of fabricated active circuit-breaker stent at three different expansion conditions.

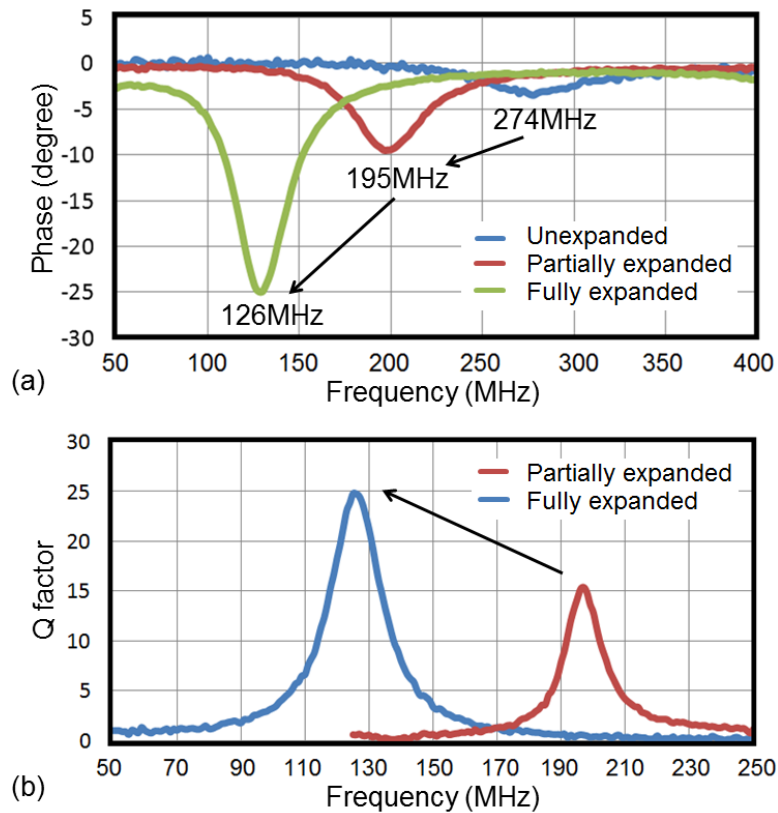


Figure 4.5: Measurement results: (a) Measured shifts of resonant dips in impedance phase of reader antenna led by expansion process, and (b) Q factors of the device recorded as a function of frequency at different expansion conditions.

4.3.3 RF heating tests

The same experimental set-up described in chapter 2 was used for characterization of RF heating and temperature regulation performance of the fabricated device. Similar to the previous test, the RF excitation was conducted with two different antenna arrangements. In one arrangement, the stent device was placed through the antenna's loop (with a circular shape) approximately at its center. In the other case, the stent device was aligned in parallel and proximity to the loop plane of the antenna; the shape of antenna in this case was adjusted to be oval, in which the longer diameter was made to be comparable

with the length of the stent device so that the antenna's loop covered almost the entire region of the device. Temporal response and frequency dependence of heating were measured in each test. The temporal responses were measured by exciting the device at resonance. To illustrate the effect of the circuit breaker in temperature regulation, the stent devices without the circuit-breaker switch were also tested to acquire reference data for comparison. The measurements were performed in air ambient for both antenna arrangements with an RF output power of 320 mW, followed by measurement in liquid environments with the parallel antenna setting using an elevated RF power.

Case 1: Device positioned through antenna loop in air

The temporal and frequency responses measured with the device before its expansion are shown in Figure 4.6(a) and 4.6(b), respectively. The same set of data acquired with the identical device after partial expansion (to 4.0 mm in diameter) are displayed in Figure 4.6(c) and 4.6(d) and those after full expansion in the artificial artery (with 6-mm diameter) are in Figure 4.6(e) and 4.6(f). Each result shows two temperature plots, one measured at the location of the highest temperature on the inductive stent and the other on the surface of the breaker chip located at an end of the device. When an RF excitation was performed with the device in the pre-expansion state (Figure 4.6(a)), both the stent and the chip were heated up to around 55 °C within ~9 seconds; once the RF signal was tuned off, device temperature gradually decreased towards the room temperature. Due to the small inductance of the stent and resultant RF power transfer, the maximum temperature reached in the device was relatively low. In particular, the breaker temperature achieved during the excitation was lower than A_s of the Nitinol (56.5 °C). Therefore, this heating process did not trigger the breaker switch, as evident from Figure

4.6(a) and 4.6(b) that show no temperature limiting effect. In contrast, the expanded device exhibited enhanced RF heating effect, due to the raised inductance of the stent, and the stent temperature became high enough to activate the breaker. IR images of the partially expanded device and those of fully expanded one (inside the artificial artery) are shown in Figure 4.7(a) and 4.7(b), respectively, each of which displays the device before RF excitation, after excitation at resonance, and after excitation off the resonance; these images indicate that heating occurred throughout the inductive stent at both partially and fully expanded cases and decreased as the field frequency shifted off from the device's f_r as expected. At resonance, the breaker temperature reached 62-63 °C, well greater than A_s of the Nitinol, due to heat transfer from the stent. The outcome of this condition is clearly visible in the results of temporal and frequency responses, showing the anticipated on-off cycles of the breaker (Figure 4.6(c) and 4.6(e)) with both partially and fully expanded cases when excited at resonance. The threshold temperatures of the cycle (switching between ~64 °C and ~50 °C) recorded in both cases match well with the measured open and close temperatures of the breaker chip noted earlier. The stent temperatures followed the cyclic patterns of the breaker's temperatures, so that stent heating was regulated within a certain temperature range during the excitation, e.g. 50-66 °C for the fully expanded case. The effect of the circuit breaker in limiting the stent temperature is evident from a comparison with the reference (in which the breaker switch was intentionally shorted), showing that the stent temperature reached ~78 °C in this case. These results indicate that the developed circuit breaker effectively clipped the stent temperature. This temperature clipping effect is also proved in the frequency responses of

heating (Figure 4.6(d) and 4.6(f)); these results show that a temperature-regulated frequency range was 15-18 MHz about the device's f_r at each expansion condition.

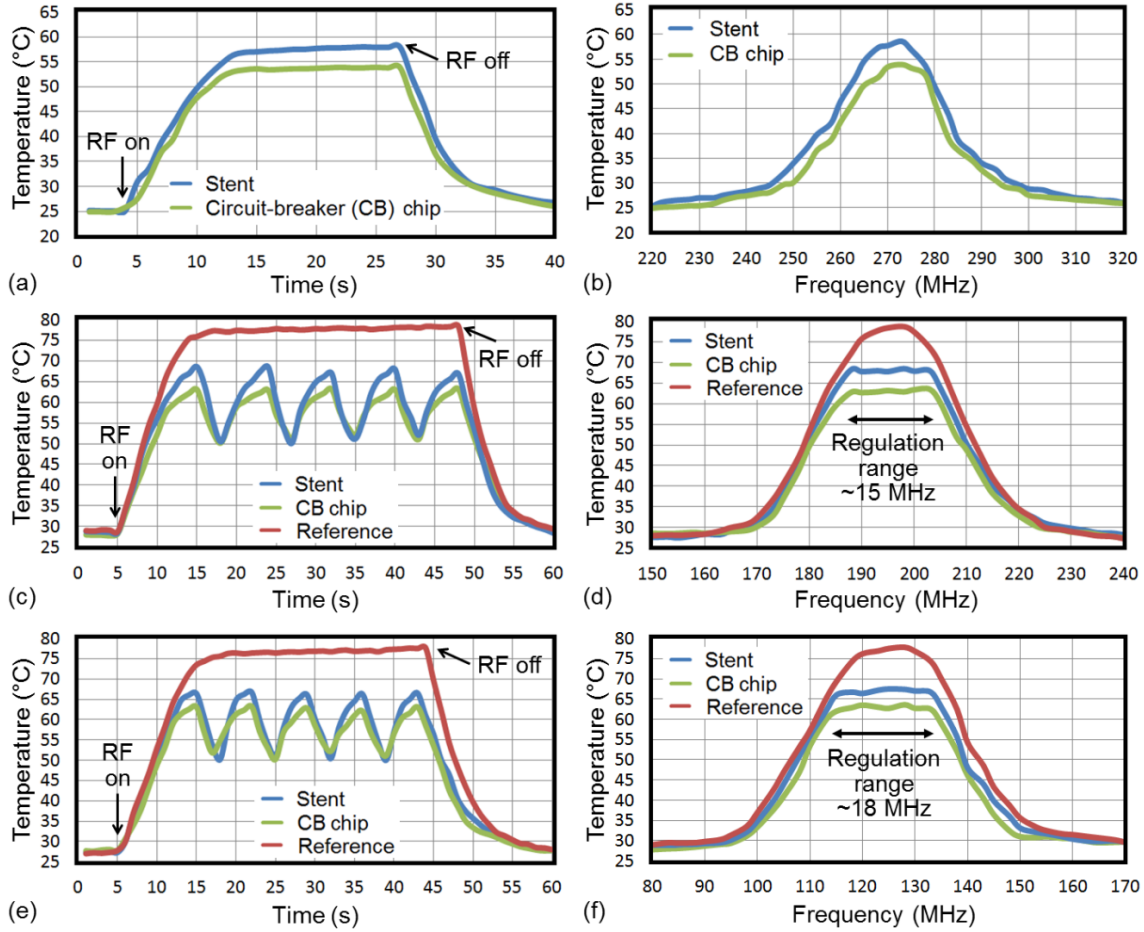


Figure 4.6: Measured temperatures of the stent device located through the antenna loop measured at the maximum temperature point of the stent as well as on the integrated circuit-breaker chip: (a) Temporal behaviour of the temperatures with RF switching and (b) generated temperatures vs. field frequency recorded with the unexpanded device; (c) and (d) those recorded with the partially expanded device; (e) and (f) those recorded with the artificial artery containing the fully expanded device. The reference data recorded without circuit-breaker function is also shown in (c)-(f).

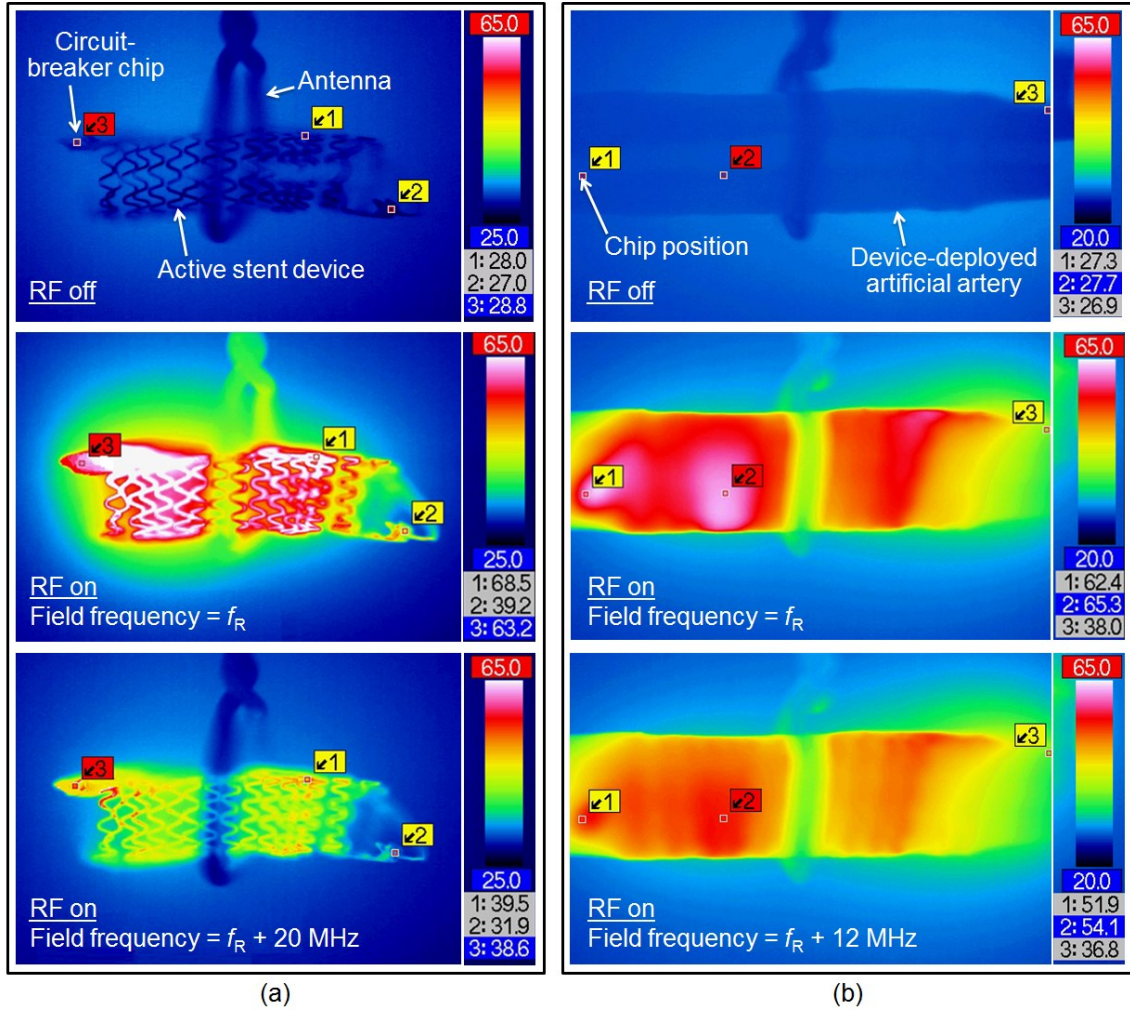


Figure 4.7: IR images of the stent device located through the antenna loop: (a) partially expanded device without RF excitation (top), with RF excitation at resonance (middle), and with RF excitation +20-MHz off the resonance (bottom); (b) artificial artery containing fully expanded device without RF excitation (top), with RF excitation at resonance (middle), and with RF excitation +12-MHz off the resonance (bottom). All RF excitations were performed with an identical RF output power (of 320 mW).

Case 2: Device positioned in parallel with antenna loop in air and liquid

The identical device at the two expansion states was tested under the other antenna setting. The same sets of measured data of temporal and frequency responses as well as IR images of the device are shown in Figure 4.8 and 4.9, respectively. The reference data

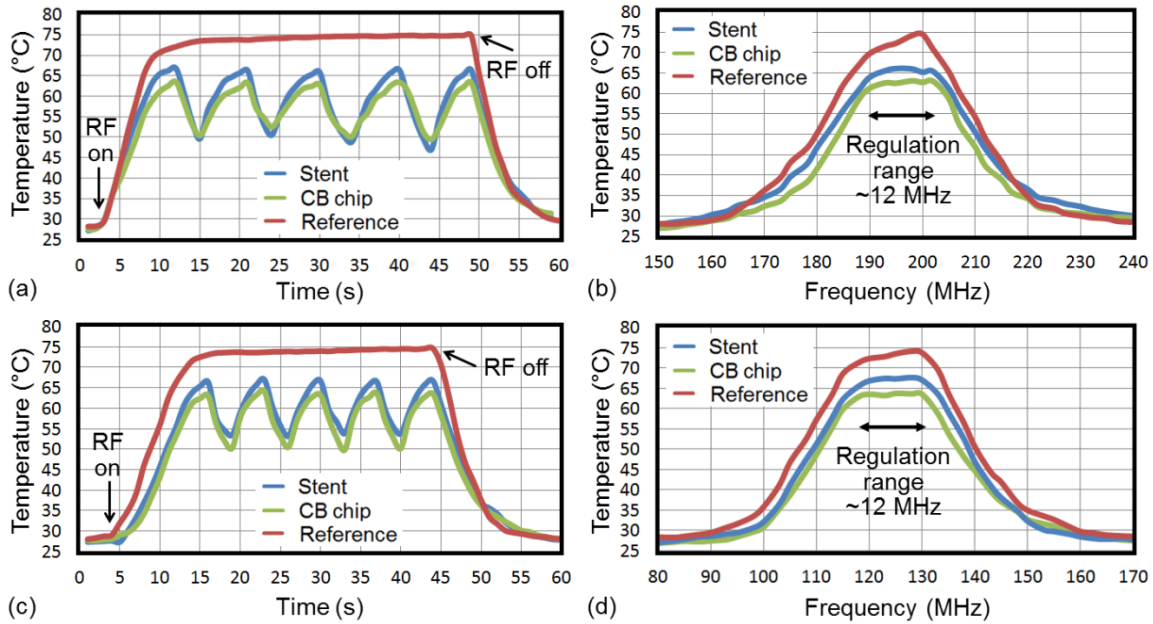


Figure 4.8: Measured temperatures of the stent device located in parallel with the antenna loop measured at the maximum temperature point of the stent as well as on the integrated circuit-breaker chip: (a) Temporal behaviour of the temperatures with RF switching and (b) generated temperatures vs. field frequency recorded with the partially expanded device; (c) and (d) those recorded with the artificial artery containing the fully expanded device. The reference data recorded without circuit-breaker function is also shown in each case.

in Figure 4.8 obtained using the device without the breaker function show that the stent's peak temperature reached $\sim 75\text{ }^{\circ}\text{C}$ in both expansion states. Note that this temperature is somewhat lower than the peak temperature observed under the same (no breaker) condition in the previous test with the other antenna setting; this is a reasonable outcome as the inductive coupling is expected to be lower in the current (parallel) antenna setting. When the breaker switch was operational (not shorted), as indicated in Figure 4.8(a) and 4.8(c), the device exhibited the on-off cycles induced by the breaker during the excitation similar to the previous results, regulating the stent temperature within a lower range (e.g., $53.6\text{-}66.5\text{ }^{\circ}\text{C}$ for the fully expanded case) than the reference level. The IR images of the partially expanded device (Figure 4.9(a)) indicate that the maximum heating occurred in

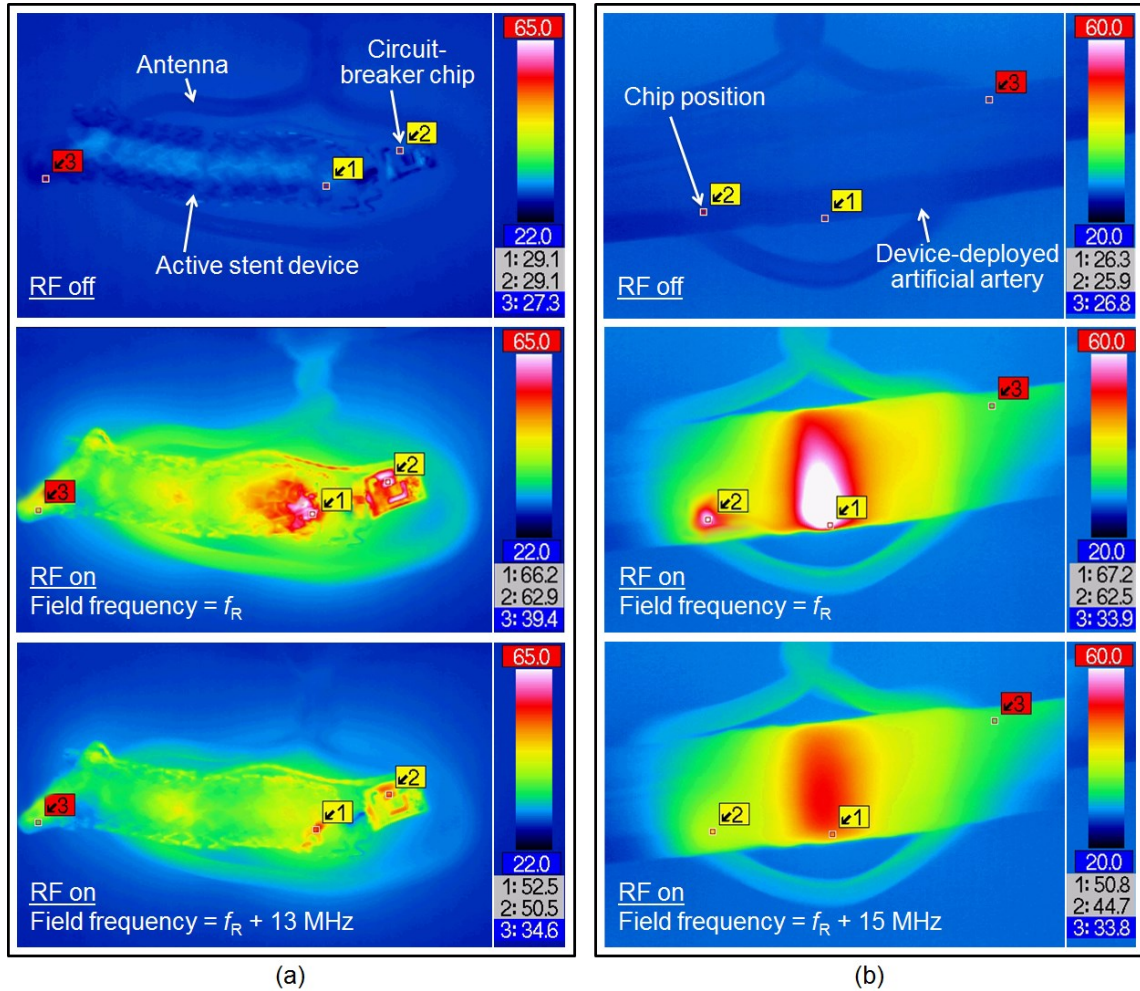


Figure 4.9: IR images of the stent device located in parallel with the antenna loop: (a) partially expanded device without RF excitation (top), with RF excitation at resonance (middle), and with RF excitation +13-MHz off the resonance (bottom); (b) artificial artery containing fully expanded device without RF excitation (top), with RF excitation at resonance (middle), and with RF excitation +15-MHz off the resonance (bottom). All RF excitations were performed with an identical RF output power (of 320 mW).

the device around the central region of the antenna loop. This phenomenon was also observed in the fully expanded device (Figure 4.9(b)); the maximum temperature on the artificial artery appeared around the antenna's central region. It is apparent from Figure 4.9 that in this parallel antenna arrangement too, heat was more effectively generated

when the field frequency was aligned to the device's f_r . Although the temperature clipping effect visible in the frequency dependence of heating (Figure 4.8(b) and 4.8(d)) is not as distinct as the previous results with the other antenna arrangement, primarily due to the lower peak temperature of the reference as noted above, the plots clearly indicate lowering of stent temperature for both expansion states leading to an approximate temperature-regulated frequency range of ~ 12 MHz.

All RF heating tests discussed previously were performed in air. In order to evaluate the heating performance in liquid ambient, the device-deployed artificial artery was filled with physiological (0.15 M) saline and excited with an output RF power of 1.26 W (the maximum available with the set-up used) under this parallel antenna set-up. For comparison, temperature distribution of the saline-filled artery tube without the device was also measured under the same RF condition as a control. Temporal temperature changes in the maximum temperature point on the active artery tube excited for 200 seconds were tracked and plotted in Figure 4.10(a) along with the result of the control. IR images of the active and control arteries upon excitation are shown in Figure 4.10(b) and 4.10(c), respectively. As apparent from Figure 4.10(a), heating needed a much longer time (180 seconds) to reach the peak temperature (~ 52 °C) compared with the case in air due to heat dissipation to the saline, an aqueous medium with higher thermal conductivity (note that water has $\sim 24\times$ larger thermal conductivity than air). As the peak temperature was lower than A_s , the circuit breaker was not activated (and thus the stent circuit was not tripped) during this heating process as can be seen in the plot. (Note that although the exact temperature of the breaker is unknown from Figure 4.10(b), it should be lower than the maximum temperature on the device as evident from Figure 4.9.) The control did not

show notable temperature change (Figure 4.10(c)), proving that heating on the artificial artery was caused by the stent device deployed inside, not by the liquid itself (a very small temperature increase (~ 1.1 °C) was detected in the control; this might have been caused by induction heating of the saline itself, a conductive liquid). The same measurements were also conducted using the identical device/artificial artery filled with de-ionized (DI) water under the same excitation conditions. The temporal responses of the active and control arteries were observed to be very close to those of the saline case shown in Figure 4.10(a), with nearly the same peak temperature achieved at a similar timing (170 seconds). Figure 4.10(d) and 4.10(e) show the IR images of the active and control arteries with DI water. It is observable from Figure 4.10(b) and 4.10(d) that the maximum heating in the device occurred at around the center region of the antenna in both saline and water filled cases, which is consistent with the results with air ambient discussed previously. An interesting observation from this comparison is that the saline-filled artery was more uniformly heated across the device compared with the water-filled one. Although the exact mechanism of this phenomenon is not clear, it might be related to the following conditions: The electrical conductivity of 0.15-M saline is $\sim 470\times$ higher than that of DI water used [33], whereas the thermal properties of these liquids are presumed to be similar [34], [35]. When surrounded by the saline, adjacent turns of the solenoid-like inductive stent are resistively coupled through capacitive dielectric layers (of Parylene C) coated on the turns, allowing certain RF current to flow through the medium between every possible pair of adjacent turns of the stent. The level of this leak current is higher when the medium is more electrically conductive, the saline case, potentially causing more direct Joule heating of the medium that elevates its temperature

(in addition to heating by the active stent) across the device. It will need careful analysis for the above hypothesis; however, the observed phenomenon of uniform heating in physiological saline is indeed a favourable effect for the targeted application of the device, which will be surrounded by blood with an electrical conductivity similar to that of the saline used in a real environment [33], [36].

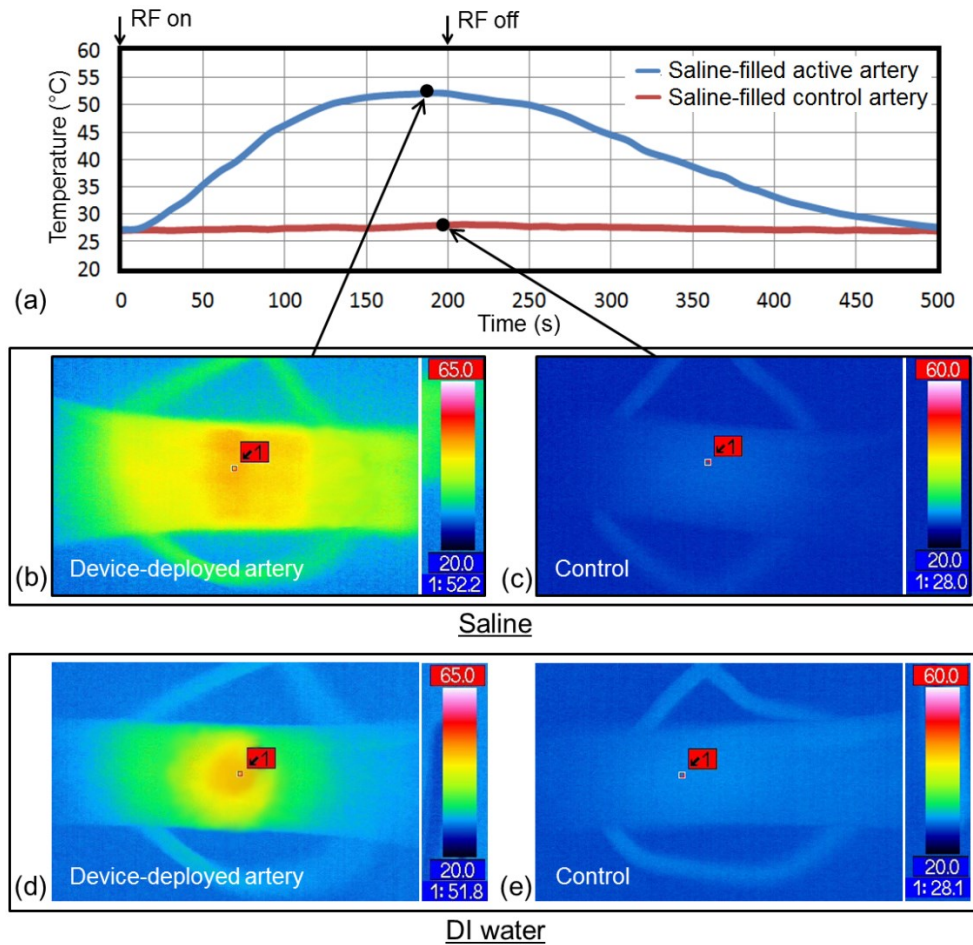


Figure 4.10: Results from wireless heating test of the active and control artificial arteries filled with liquid and RF excited: (a) Temporal thermal behaviours of the arteries filled with 0.15-M saline excited for 200 seconds; (b) and (c) IR images of the saline-filled active and control arteries, respectively, under RF radiation at 1.26-W output power (the timings that these images were recorded are indicated in (a) with arrows); (d) and (e) those of the DI-water-filled active and control arteries, respectively, under the same RF radiation.

Chapter 5

Conclusion and Future Outlooks

This chapter concludes the results of the entire study discussed in this thesis. This is followed by a summary of the original contributions made in this research project and also original objectives achieved during my master program. Suggestions for further device development and directions for future research are also stated.

5.1 Conclusion

This thesis describes all my research works done during the program. Firstly, a novel electrothermal stent has been studied and experimentally demonstrated in preliminary tests. A prototype device was constructed by integrating a lithographically fabricated flexible capacitor strip with a stainless-steel inductive stent to form a resonant circuit. The stent device was shown to function as a frequency-dependent wireless heater controllable using external RF field through its frequency tuning. The device design was arranged to enable electrical and mechanical deployment inside an artificial artery using a commercial angioplasty balloon. RF excitation of device was tested under two different spatial arrangements of active stent with respect to the transmitting loop antenna, i.e., the stent through the loop and that parallel to the loop, both of which showed rapid heating and its strong dependence on operating frequency. Comparison of heating behaviours indicated that the expanded device produced heat more efficiently than the unexpanded device, presumably due to enhanced inductive coupling and power transfer led by $>2\times$ inductance of the fully expanded device. The device expanded in artificial artery tube was

revealed to provide temperature rise of 30 °C or more on the tube walls, well above the targeted maximum temperature rise of 13 °C, when radiated with an RF field whose frequency was tuned to resonate the device. The obtained results prove the essential functionality of the device toward endohyperthermia therapy applications.

Secondly, a biocompatible circuit breaker device has been designed, fabricated, and demonstrated experimentally with a focus on its application to electronic medical implants, including the active stent targeted in this thesis. The device design was centered on a micromachined Nitinol cantilever actuator that was used as a miniaturized, normally-closed thermoresponsive switch for opening/closing a circuit of interest depending on heating condition of the circuit in a passive manner. FEA was used to determine the design of the cantilever actuator and its cold-state bending to ensure a firm contact of the cantilever tip with the counter electrode patterned on the substrate. The circuit breaker was fabricated with a combination of μ EDM and lithography-based processes and Ti packaged in a form of chip. The fabricated breaker chip was measured to have a cold-state resistance of 14 Ω and enter the fully open state at a chip temperature of 63 °C. The self-heating effect was characterized for the fabricated chip to evaluate its maximum current allowance with both DC and RF signals. The designed function of the developed breaker was successfully demonstrated by coupling it with a circuit platform of wireless RF resonant heater, showing that the original heater temperature of >90 °C was well regulated within ~50 °C through a self-sustained switching behaviour of the breaker. These results verify the intended functionality of the developed breaker device as a safety temperature limiter.

Finally, an electrothermally active stent device with a temperature regulation feature has been developed and demonstrated experimentally. The developed circuit-breaker chip served as a temperature-sensitive switch to enable reversible breaking of the wireless heater circuit constructed using the inductive stent, regulating the stent temperature within a certain range under RF excitation. The breaker chip was also developed to embed a capacitor element so that the integration of the chip with the stent establishes the resonant heating circuit with series-connected breaker switch. Microfabricated proof-of-concept prototypes were successfully tested to show the intended temperature regulation enabled by the integrated circuit breaker in an open loop and fully passive manner. RF heating of the stent device in liquid environment was demonstrated using device-deployed artificial arteries filled with physiological saline as well as with DI water. The results revealed a notable difference in heating performance between the cases with the saline and water, showing more uniform heating with the saline, a favourable finding for the target application; a potential cause of this phenomenon was proposed. These experimental results indicate the feasibility of arterial RF heating in liquid ambient through the active stent, with the circuit breaker to automatically limit the absolute temperature of the stent within a designed threshold, representing a promising step to advancing stent technology toward realizing clinically practical, safe endohyperthermia therapy for inhibition and management of in-stent restenosis.

5.2 Contributions

1. Design and demonstration of an active stent device with selective RF heating capability. By integrating with an external capacitor to form a *LC* circuit, this

active stent device is proposed for solving artery re-narrowing caused by restenosis after device implantation.

2. Design and fabrication of a novel thermal sensitive MEMS circuit-breaker chip. This MEMS chip is assembled with bio-compatible materials, and takes actuation according to the device temperature. When under low temperature, the chip is electrically conductive from top to bottom. Once heated up above the temperature threshold, chip actuates and turns to be electrically non-conductive from its top to bottom.
3. Design and demonstration of an active stent device with a feature of temperature regulation. By integration the circuit breaker chip with a capacitor to the stent, device temperature becomes manageable under RF excitation. With the circuit-breaker chip actuation, device internal circuitry opens or closes, limiting device temperature within certain range and prevent device from overheating. Device also has been evaluated *in-vitro* for its clinical potential, showing its potential capability of working under biological environment.

5.3 Future outlooks

For future research work on this subject, following suggestions are proposed for development directions.

1. Further device *in-vitro* tests are needed. Currently, the device RF heating has been verified within types of liquid sealed inside artificial arteries. To evaluate device RF heating performance after implantation, an *in-vitro* test with liquid flows should be considered. Device RF heating profile changes with different

liquid flows passing through the artery tubes, producing results closer to the real physiological situation.

2. Studies on further device miniaturization and optimization. Smaller size of chip can significantly reduce the space occupation, providing convenience for stent expansion and lower invasiveness to body when perform device implantation as well as product material costs. Also, instead of using rectangular shape of chip packaging, other shape formations could be considered to prevent possible injuries from device sharp edges.
3. The adjustment of the open temperature of the breaker chip (to be ~ 50 °C). This can be addressed simply by using a Nitinol material with a suitable austenitic-phase temperature for the switch fabrication.
4. The enhancement of the Q factor of the device. This will be a direct path to improving the RF-to-thermal power conversion and thus heating efficiency; one effective method to achieve this goal is to coat the inductive stent with a thin film of highly conductive metal as discussed. The optimization of the RF transmission system and antenna will be another important aspect towards the same goal.
5. Although the current device has been proved capable working within blood-like environment, *in-vivo* test is mandatory for further verification. The device performance should be evaluated with actual blood flow within a blood vessel to see effective thermal generation and conduction, while the RF antenna used for device excitation is outside with the higher bandwidth availability [37].

Bibliography

- [1] A.G. Logan and D. Bradley, "Sleep Apnea and Cardiovascular Disease," *Curr. Hypertens. Rep.*, vol.12, pp.182-190, 2010.
- [2] D. Stoeckel, A. Pelton, T. Duerig, "Self-Expanding Nitinol Stents: Material and Design Considerations," *Eur. Radiol.*, vol. 14, pp. 292-301, 2004.
- [3] H.W. Roberts, S.W. Redding, "Coronary Artery Stents: Review and Patient-Management Recommendations," *J. Am. Dent. Assoc.*, vol. 131, pp. 797-801, 2000.
- [4] National heart, lung, and blood institute. (2014, June 5). *What is coronary angioplasty?* [Online]. Available: <http://www.nhlbi.nih.gov/health/health-topics/topics/angioplasty/during.html>
- [5] *Macerick PTCA Dilatation Catheter User Guide*, Boston Scientific Corporation., Boston, MA, 2011.
- [6] M.R. Bennett, "In-Stent Stenosis: Pathology and Implications for the Development of Drug Eluting Stents," *Heart*, vol. 89, pp. 218-224, 2003.
- [7] V. Rajagopal, S.G. Rockson, "Coronary Restenosis: A Review of Mechanisms and Management," *Am. J. Med.*, vol. 115, pp. 547-553, 2003.
- [8] J. Moses et al, "Sirolimus-Eluting Stents versus Standard Stents in Patients with Stenosis in a Native Coronary Artery," *The New England Journal of Medicine*, vol. 349(14), 2003, pp. 1315 - 1323.
- [9] G. Stone et al., "One-Year Clinical Results with Slow-Release, Polymer-Based, Paclitaxel-Eluting TAXUS Stent: The TAXUS-IV Trial," *Circulation*, vol. 109, 2004, pp. 1942 - 1947.
- [10] T. Luscher et al., "Drug-Eluting Stent and Coronary Thrombosis: Biological Mechanisms and Clinical Implications," *Circulation*, vol. 115, 2007, pp. 1051 - 1058.
- [11] C. Brasselet, E. Durand, F. Addad, F. Vitry, G. Chatellier, C. Demerens, M. Lemitre, R. Garnotel, D. Urbain, P. Bruneval, A. Lafont, "Effect of Local Heating on Restenosis and In-Stent Neointimal Hyperplasia in the Atherosclerotic Rabbit Model: A Dose-Ranging Study," *Eur. Heart J.*, vol. 29, pp. 402-412, 2008.
- [12] R. Tan, T. McClure, C.K. Lin, et al. "Development of a fully implantable wireless pressure monitoring system," *J. Biomedical microdevices*, vol. 11, pp. 259-264, 2009.

- [13]F. Albano, Y.S. Lin, D. Blaauw, et al., "A fully integrated microbattery for an implantable microelectromechanical system," *Journal of Power Sources*, vol. 185, pp. 1524-1532, 2008.
- [14]G.D. Dangas, B.E. Claessen, A. Caixeta, E.A. Sanidas, G.S. Mintz, R. Mehran, "In-Stent Restenosis in the Drug-Eluting Stent Era," *J. Am. Coll. Cardiol.*, vol. 56, pp. 1897-1907, 2010.
- [15]M.S. Mohamed Ali, B. Bycraft, A. Bsoul, K. Takahata, "Radio-Controlled Microactuator Based on Shape-Memory-Alloy Spiral-Coil Inductor," *J. Microelectromech. Syst.*, vol. 22, pp. 331-338, 2013.
- [16]S. Rahimi, E.H. Sarraf, G.K. Wong, K. Takahata, "Implantable Drug Delivery Device Using Frequency-Controlled Wireless Hydrogel Microvalves," *Biomed. Microdev.*, vol. 13, pp. 267-277, 2011.
- [17]Chemistry for Biologists. (2014, June 10).*Enzymes* [Online]. Available: <http://www.rsc.org/Education/Teachers/Resources/cfb/enzymes.html>
- [18]Y. Luo, M. Dahmardeh, X. Chen and K. Takahata, "Selective RF heating of resonant stent toward wireless endohyperthermia for restenosis inhibition," *Proc. IEEE Int. Conf. Micro Elec. Mech. Syst.*, San Francisco, USA, 2014, pp. 877-880.
- [19]A.R. Mohammadi, M.S.Mohamed Ali, D. Lappin, C. Schlosser, K. Takahata, "Inductive Antenna Stent: Design, Fabrication, and Characterization," *J. Micromech. Microeng.*, vol. 23, 025015, 2013.
- [20]M.S. Mohamed Ali and K. Takahata, "Frequency-controlled wireless shape-memory-alloy microactuators integrated using an electroplating bonding process," *Sensors and Actuators A: Phys.*, vol. 163, pp. 363-372, 2010.
- [21]S.D. Senturia, *Microsystem Design*, Kluwer Academic Publishers, New York, 2001.
- [22]M.S. Mohamed Ali, W.N. Yuan and K. Takahata, "Analysis of Micropatterned Wireless Resonant Heaters for Wireless-Control of MEMS Thermal Actuators," *Microsystem Technologies*, Vol. 20, pp. 235-241, 2014.
- [23]D. Lappin, A.R. Mohammadi, K. Takahata, "An Experimental Study of Electrochemical Polishing for Micro-Electro-Discharge-Machined Stainless-Steel Stents," *J. Materials Science: Materials in Medicine*, vol. 23(3), pp. 349-356, 2012.
- [24]V. Sridhar and K. Takahata, "A Hydrogel-Based Passive Wireless Sensor Using a Flex-Circuit Inductive Transducer," *Sensors and Actuators A: Physical*, vol. 155, pp. 58-65, 2009.

- [25]J. Mai, L. Peng, Z. Lin and X. Lai, “Experimental Study of Electrical Resistivity and Flow Stress of Stainless Steel 316L in Electroplastic Deformation,” *Mater. Sci. Eng. A*, vol. 528, pp. 3539-3544, 2011.
- [26]E.R. Adair, and R.C. Petersen, “Biological effects of radiofrequency/microwave radiation,” *IEEE Transactions on Microwave Theory and Techniques*, vol. 50, pp. 953-962, 2002.
- [27]M.S. Mohamed Ali and K. Takahata, “Wireless microfluidic control with integrated shape-memory-alloy actuators operated by field frequency modulation.” *J. Micromech. Microeng.*, vol. 21, 2011.
- [28]T.W. Jau, “RF MEMS switches: High-frequency performance and hot-switching reliability,” *High Freq. Electron.*, pp.32–38, 2013.
- [29] J. Ryhanen, “Biocompatibility of Nitinol,” *Min. Invas. Ther. & Allied Technol.*, vol. 9, pp.99-106, 2000.
- [30]M.E. Souni and H.F. Brandies, “Assessing the biocompatibility of NiTi shape memory alloys used for medical applications,” *Anal. Bioanal. Chem.*, vol. 381, pp.557–567, 2005.
- [31]R.R. Richardson, J.A. Miller and W.M. Reichert, “Polyimides as biomaterials: Preliminary biocompatibility testing,” *Biomaterials*, vol. 14, pp. 627–635, 1993.
- [32]J.M. Seo, S.J. Kim, H. Chung, E.T. Kim, H.G. Yu and Y.S. Yu, “Biocompatibility of polyimide microelectrode array for retinal stimulation,” *Mater. Sci. Eng. C*, vol. 24, pp. 185–189, 2004.
- [33]X. Chen, D. Brox, B. Assadsangabi, Y. Hsiang and K. Takahata, “Intelligent Telemetric Stent for Wireless Monitoring of Intravascular Pressure and Its *In-vivo* Testing,” *Biomedical Microdevices*, vol. 16, pp. 745-759, 2014.
- [34]I. Martinez. (2014, Dec.). Properties of Some Particular Solutions, Ciudad Universitaria, Spain. [Online]. Available: <http://webserver.dmt.upm.es/~isidoro/bk3/c07sol/Solution%20properties.pdf>
- [35]C. Tangwonsan, L. Chachati, J.G. Webster and P.V. Farrell, “*In-vitro* Calibration of a System for Measurement of *In-vivo* Convective Heat Transfer Coefficient in Animals,” *Biomedical Engineering Online*, vol. 5, 2006, DOI: 10.1186/1475-925X-5-57.
- [36]S.N. Mohapatra, K. L. Costeloe and D.W. Hill, “Blood Resistivity and Its Implications for the Calculation of Cardiac Output by the Thoracic Electrical Impedance Technique,” *Intens. Care. Med.*, vol. 3, pp. 63-67, 1977.

- [37]G. C. Crumley, N. E. Evans, J. B. Burns, and T. G. Trouton, “On the design and assessment of a 2.45 GHz radio telecommand system for remote patient monitoring,” *Med. Eng. Phys.*, vol. 20, pp. 750–755, 1999.